Low-Temperature Atmospheric Pressure Plasma Processes for "Green" Third Generation Photovoltaics

Davide Mariotti,* Thierry Belmonte, Jan Benedikt, Tamilselvan Velusamy, Gunisha Jain, Vladimir Švrček

Atmospheric pressure plasmas (APPs) have achieved great scientific and technological advances for a wide range of applications. The synthesis and treatment of materials by APPs have always attracted great attention due to potential economic benefits if compared to low-pressure plasma processes. Nonetheless, APPs present very distinctive features that suggest atmospheric pressure operation could bring other benefits for emerging new technologies. In particular, materials synthesized by APPs which are suitable candidates for third generation photovoltaics are reviewed here.

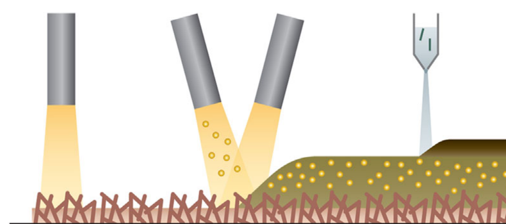

1. Introduction

Non-equilibrium, or low-temperature, low-pressure plasma processes have had great success in materials processing as key enablers to the unparalleled success of the microelectronic and semiconductor industry, the antechamber to today photovoltaic (PV) technology. There is no doubt that without low-pressure plasma processing, today's solar panels would be even more prohibitive, raising our current obstacles for introducing PV in the consumer market. In recent years, there has been tremendous interest in developing technologies that would allow attaining the same low-pressure plasma processing capabilities at atmospheric pressure. Generating plasmas at atmospheric pressure, however, can quickly reveal non-trivial challenges where the control and characteristics of low-pressure processes may be lost or difficult to realize. Nonetheless, low-temperature atmospheric pressure plasmas (APPs) have achieved great progress in the past decade with impressive technological advancements.[1,2] APPs have enabled the advent of plasma medicine,[2,3] for instance, and have fueled a vast range of opportunities at all technological readiness levels. While materials processing, in the sense intended by the semiconducting industry, may have been one of the main drivers for APP research, APP materials processing has probably been lagging behind all other APP technological developments.

One of the reasons for this may have been the misplacement of expectations and that APPs were not destined to replace low-pressure plasmas but to offer a solution to new challenges. The advent of nanotechnology and the necessity of advanced functional materials for next generation photovoltaics may represent this challenge and become the opportunity for APPs to shine. Future

D. Mariotti, T. Velusamy, G. Jain
Nanotechnology and Integrated Bio-Engineering Centre (NIBEC), Ulster University, Newtownabbey, UK
E-mail: d.mariotti@ulster.ac.uk
T. Belmonte
Ruhr-Universität Bochum, D-44780 Bochum, Germany
J. Benedikt
CNRS, Institut Jean Lamour, UMR CNRS 7198, Nancy F-54042, France
V. Švrček
Research Center for Photovoltaic, National Institute of Advanced Industrial Science and Technology (AIST), Central 2, Umezono 1-1-1, Tsukuba 305-8568, Japan
This is an open access article under the terms of the Creative Commons Attribution License, which permits use, distribution and reproduction in any medium, provided the original work is properly cited.

Plasma Process. Polym. **2016**, *13*, 70–90
© 2016 The Authors. *Plasma Processes and Polymers* published by Wiley-VCH Verlag GmbH & Co. KGaA Weinheim
wileyonlinelibrary.com

DOI: 10.1002/ppap.201500187

16128869, 2016, 1, Downloaded from https://onlinelibrary.wiley.com/doi/10.1002/ppap.201500187 by Technische Informationsbibliothek, Wiley Online Library on [24/01/2025]. See the Terms and Conditions (https://onlinelibrary.wiley.com/terms-and-conditions) on Wiley Online Library for rules of use; OA articles are governed by the applicable Creative Commons License

generation of solar cells will require fast and low-cost materials processing schemes, capable of delivering a wide range of materials with nanoscale features. As we cannot expect APPs to deliver all the fabrication needs, it is clear that some of the requirements for the fabrication of future PV devices may be met by some of the strongest features of APP materials processing.

In this contribution, we will argue the versatility of APPs for the fabrication of a wide range of materials, which, at this present time, can be considered good candidates for high efficiency next generation solar cells. In particular, we will focus on materials that are being studied for third generation (3-Gen) PVs, highlighting corresponding APP processing capabilities. We will first introduce 3-Gen PVs with a generalized device structure and we will then describe APP technologies and configurations. Following, progress in the synthesis of specific materials will be outlined and discussed. The article will then be completed with examples of APPs used to improve PV devices.

2. Third Generation Photovoltaics (PVs)

The basic idea of 3-Gen PVs is to significantly increase device efficiencies beyond theoretical predicted limits (~30% for single absorber devices[4]) while maintaining manufacturing costs low as for 2-Gen thin film technologies. The environmental impact is also important for 3-Gen PVs whereby abundant and non-toxic materials have to be preferred.

The efficiency increase can be achieved mainly by tackling two main issues that negatively impact solar energy conversion. Firstly, solar radiation photons with energy E_{ph} smaller than the energy bandgap of the active layer materials (E_g) are not absorbed and therefore cannot be utilized for carrier generation. Secondly, the excess energy of absorbed photons with E_{ph} larger than the bandgap is lost due to thermalization of the generated electron–hole pairs. These fundamental spectral losses in a single-junction silicon solar cell, for instance, can be as large as 50%.[5] In principle, 3-Gen PV technologies can overcome these fundamental limitations of photon to electron conversion, thus improving both efficiency and lowering the costs.

Within the scope of 3-Gen PVs, several routes have been proposed such as the development of multi-junction solar cells,[6] intermediate bandgap solar cells,[7] multiple-exciton generation solar cells,[8] quantum dot solar cells under one sun and with concentrators,[9] solar cells using down- and up-conversion principles,[10] and down-shifters.[11] In the last decade, research in 3-Gen PV technologies have achieved impressive result, however, where efficiency improvements could be achieved, costs were failing to meet economic requirements and vice versa. For instance, high-efficiency multi-junction solar cells are still too expensive while devices based on quantum dots, which can potentially be deployed at very low-cost, still present very low efficiencies (<10%). Furthermore, quantum dots devices currently fail to meet environmental requirements as toxic or rare materials are often used (e.g., Pb, Se, etc.). Nonetheless, the use of quantum dots in solar cells remains one of the most promising avenues to avoid thermalization losses, in particular through mechanisms of carrier multiplication (CM), where a single photon absorbed in the active layer could generate multiple pairs of electrons and holes.[4,12] Silicon quantum dots, also called silicon nanocrystals (Si NCs), are very attractive within this context and initial fundamental results on Si NCs were very promising. Multiple-exciton generation, a type of CM, was demonstrated in Si NCs and the absorption of a single high-energy (>3 eV) photon was shown to generate more than two electron–hole pairs.[13] CM in Si NCs was also confirmed through space-separate quantum cutting, a second type of CM.[14] The successful implementation of CM mechanisms could in principle shift the efficiency theoretical limit to ~45%[13] for single absorbers.

Low-temperature APP technologies could play a crucial role in enabling 3-Gen PVs. APPs offer a range of advantageous characteristics capable of sustaining, initially, the fundamental research and then offer methodologies for industrial implementation. APPs are versatile, low-cost and, as it will be demonstrated throughout this paper, they can produce the full range of materials required for 3-Gen PV device fabrication. Although several device architectures and different fundamental mechanisms can be exploited for 3-Gen PVs, here we will exemplify APP processing capabilities with reference to a general and simplified device structure which relies on quantum dots (QDs) to absorb light and produce carriers (Figure 1). On this basis, it will then be easy to extend the integration of APP processes for other 3-Gen device architectures and

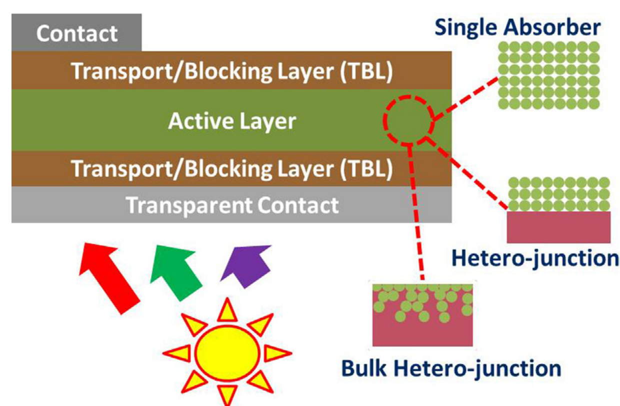

Figure 1. A general schematic structure of a third generation photovoltaic device based on quantum dots.

© 2016 The Authors. *Plasma Processes and Polymers* published by Wiley-VCH Verlag GmbH & Co. KGaA Weinheim

16128869, 2016, 1, Downloaded from https://onlinelibrary.wiley.com/doi/10.1002/ppap.201500187 by Technische Informationsbibliothek, Wiley Online Library on [24/01/2025]. See the Terms and Conditions (https://onlinelibrary.wiley.com/terms-and-conditions) on Wiley Online Library for rules of use; OA articles are governed by the applicable Creative Commons License

mechanisms. It should be noted that 3-Gen PVs is still a technology at very low technology readiness levels, therefore materials fabrication processes will be mainly discussed in the context of enabling PV research and not necessarily to demonstrate industrial manufacturing; however, we will argue the potential of industrial scalability. As a consequence, APP processes should be compared to other material fabrication technologies that are also mainly utilized in a research setting. With these premises, a general 3-Gen generalized device structure can be described as in Figure 1.

The structure in Figure 1 includes top and bottom contacts, which are generally made of either a metal thin layer or a conductive optically transparent material. The function of these materials is merely to collect carriers; however, their work-functions have to be suitably aligned with the rest of the device structure. The bottom contact generally needs to be transparent to allow for the light to be absorbed in the active layer; a non-transparent-patterned bottom contact is also possible if a very low resistivity material is used. Transparent conductive oxides (TCO) are very common materials for bottom contacts and in particular indium-tin oxide (ITO) or fluorine-doped tin oxide (FTO) are widely used. Transport and blocking layers (TBLs) are optional components but are being increasingly used in 3-Gen architectures as they largely reduce interface recombination of carriers. These are generally wide bandgap oxides that allow either electrons or holes to be collected (transport function) while opposing a large energy barrier for the carrier with opposite sign (blocking function). Also for TBLs, suitable alignment of energy band levels is very important for the overall device performance. Finally, the active layer is designed to absorb light and produce uncorrelated electron–hole pairs. Active layers based on quantum dots can be generally classified in three different configurations: single absorber, single-junction or bulk hetero-junction. In a single absorber, carrier generation rely on the QDs only and dissociation is expected to occur due to strong internal electric fields within the absorber or at the interfaces with corresponding TBLs. A single-junction active layer takes advantage of complementary absorption from a second material which is also expected to produce a dissociating junction at the interface with the QDs. Transport is one of the main drawbacks of QDs systems as carriers are easily lost at interfaces; in order to alleviate this problem, bulk heterojunction have been devised which try to reduce the transport path to a dissociating interface and to the collecting contacts or TBLs. Bulk hetero-junction requires a material capable of interpenetrating with the QDs architecture so that polymers are often used in this case.

However, transport issues do remain one of the major hurdles to implement efficient 3-Gen devices, not just in the active layer. The use of nanostructured materials introduces interfaces throughout the device structure which can easily increase chances of defects formation during either the synthesis process or during the integration of the nanomaterials in the device structure. Clearly, this is an intrinsic challenge that is not necessarily linked to one or another fabrication process; rather it is closely related to the concepts of 3-Gen PVs. Defects and dangling bonds at the QD surfaces can introduce a large density of mid-gap and band-tail trap states. It follows that transport in 3-Gen devices is not a trivial issue, however, it should not be overestimated as a few different factors do contribute to mitigate the negative impact of a large number of interfaces. Firstly, nanoscale materials and in particular QDs tend to exhibit highly pure "inner cores" due to thermodynamic stability, so that if defects are present these tend to remain at the surface. This was, for instance, observed in the synthesis of Si QDs, whereby the introduction of even very small amount of hydrogen in the core (not at the surface) can determine the amorphous versus crystalline nature of the QD.[15] Secondly, defects at the surface are easier to address with a range of surface treatments, which can achieve superior passivation and eliminating most defects and dangling bonds.[16–18] There are also aspects that relate to the device architecture and in particular it should be noted that mobility requirements, e.g., first generation PVs are far higher than those for 3-Gen devices, due to the absorber layer expected to be order of magnitudes thinner in the latter ones. Furthermore, the use of nanomaterials and 3-Gen concepts allows for some flexibility in designing novel device architectures which can largely reduce collection paths or rely on different transport mechanisms which maybe more efficient (e.g., tunneling, intra-band formation, etc.).

3. Atmospheric Pressure Plasma Technologies

3.1. General Features of APPs

Non-thermal APPs have been considered an alternative to low pressure plasmas where heat- or vacuum-sensitive surfaces have to be treated (e.g., polymers, wood, liquids, living tissues). Additionally, the fact that APPs can be operated without expensive vacuum-related equipment and at lower powers, make their application an attractive cost effective alternative to low-pressure plasmas. However, if a chamber for controlled atmosphere is needed and/or the plasma is operated with a high gas flow,[19,20] their cost-effectivity can be reduced significantly. Atmospheric pressure conditions limit also the range of possible applications. Large gas density and high collisional rates result in strongly collisional plasma sheaths, where the ions cannot be accelerated as it is the case of low pressure plasmas. Very likely, this impacts and generally prevents

© 2016 The Authors. Plasma Processes and Polymers published by Wiley-VCH Verlag GmbH & Co. KGaA Weinheim
DOI: 10.1002/ppap.201500187

the possibility of utilizing ion bombardment at atmospheric pressure, which is in many cases beneficial for the properties of thin films. However, ion bombardment at atmospheric pressure is still in discussion and there maybe conditions at which this could be enhanced and exploited for the optimization of film properties.[21–23] While low-pressure plasma all tend to maintain a low-temperature, APPs offer opportunities to vary the gas temperature from room temperature to high temperatures which can be used for localized surface post-treatment in the form of annealing of the thin film.[24–27] The geometry of the plasma system is also important as for example the electrode distance in capacitively coupled plasmas, can be used to tune the electron energy distribution function, and with that the plasma chemistry.[28,29]

In general, the generation of non-equilibrium conditions under APPs is a challenge. The high collisional rates are favorable for equilibrating the temperatures between electrons and heavy particles leading to arc formation. Additionally, several thermal instabilities[30] lead to plasma filamentation. Special plasma-generation schemes have to be used to achieve non-equilibrium conditions, where the main goals are to suppress gas heating and limit discharge currents. This can be achieved by small plasma volume (so-called microplasmas, with cooling achieved by large surface-to-volume ratio), high gas flows (plasma jets), use of helium (lowest collision cross-section, very high heat conductivity), pulsed operation (short times limit the gas heating), alternate current (AC) operation, and dielectric barriers that prevent direct currents (DCs) or high frequency operation (radio frequency driven discharges up to microwave driven discharges).[31–35] Most of APP reactors combine together several of these features.

Plasma filamentation (streamers) still appears in many APPs and it usually has negative effect on the homogeneity of the plasma treatment or the grown material. Complete suppression of APP filamentation results from careful tuning of plasma conditions and following the same principles as listed above, i.e., use of gas mixture (e.g., helium with small admixture of precursor gas), carefully selected plasma operation mode (e.g., with dielectric barriers and the plasma operated in the Townsend mode[36]), or controlled pulsing scheme.[37] The recombination rates of reactive species and ions are also correspondingly high, which can cause problems by transport of reactive species to the place of treatment and which leads in many cases to unwanted nanoparticle formation in the gas phase. At the same time, these characteristics are particularly suited for fast nucleation and growth of nanomaterials.

3.2. APPs for Material Synthesis

APP reactors for the synthesis of thin films, nanostructured films, or in-flight gas phase nanoparticle generation have to overcome the limitations mentioned in the previous section. First, transport of precursor molecules and reactive species is mainly governed by convection as diffusion is very slow. This has to be considered in the design of the plasma reactor. The gas transport through convection has to bring enough precursor gas into the active plasma zone or in the plasma afterglow, it has to limit gas residence time (avoiding vortexes where particles can be formed in unreliable manners)[38,39] and it should prevent or minimize material formation inside the plasma reactor walls (approaches such as gas shrouds[40] or substrates on both electrodes[41,42] are used). Several and for sure not comprehensive examples of possible designs of APPs for material synthesis are schematically presented in Figure 2.

The deposition approaches can be divided into two main groups. First, localized treatment can be achieved by APP jets or plasma torches, where the deposition usually results in an axially symmetric bell-shaped or ring-shaped profile on a few mm^2 or cm^2,[43–46] see Figure 2b, d, and e. The deposition area can be increased by using gas showers with deposition area of few cm^2 as it is done in a commercial reactor (Atomflo, see Figure 2f).[47–50] Homogeneous film growth over larger area can be achieved by using linear plasma jet arrays with overlapping treatment areas (see Figure 3), combined with movement of the substrate, or by movement of the plasma reactor in a two-dimensional pattern over the treated surface. The APP jets mounted on a robotic arm can also be used to treat more complex three-dimensional objects.

An alternative is the use of dielectric barrier discharges (DBD) with planar large area electrodes or slit reactors (see Figure 2a and c), both combined with translational movement of the surface in one direction. The substrate movement is needed even in the case of DBDs with large electrode area, because the film homogeneity is given only in the direction perpendicular to the gas flow.[39] The scalability of these discharges in one direction is currently the most promising approach for treatment of large flat areas by APPs. An example of a large-area thin film deposition on foils at atmospheric pressure is shown in Figure 4.

An alternative method leading to patterned coating or surface modification of two- and three-dimensional substrates is a so-called plasma printing.[51] It can be applied where only very thin films are needed and where they should not cover the whole area of the substrate, but should be patterned with feature size starting at few hundreds of micrometers. The powered electrode in plasma printing is a structured stamp, which is placed on the substrate (grounded electrode). The stamp structuring restricts the volume, where the plasma is generated, limiting hence the deposition or plasma treatment to plasma facing areas. The deposition stops after the precursor gas is consumed, but several schemes exist with active gas supply into the

© 2016 The Authors. *Plasma Processes and Polymers* published by Wiley-VCH Verlag GmbH & Co. KGaA Weinheim

16128869, 2016, 1, Downloaded from https://onlinelibrary.wiley.com/doi/10.1002/ppap.201500187 by Technische Informationsbibliothek, Wiley Online Library on [24/01/2025]. See the Terms and Conditions (https://onlinelibrary.wiley.com/terms-and-conditions) on Wiley Online Library for rules of use; OA articles are governed by the applicable Creative Commons License

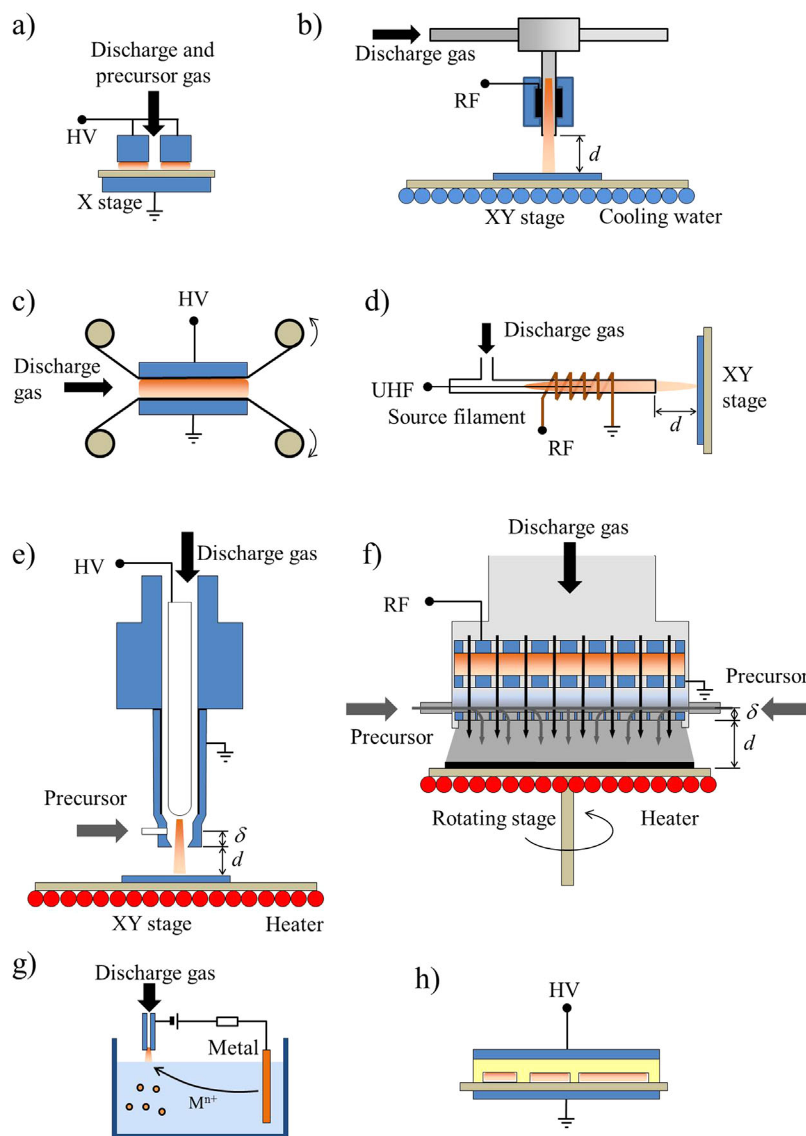

Figure 2. Selected examples of atmospheric pressure plasma (APP) configurations used for deposition or surface treatment. (a) Dielectric barrier discharge (DBD) from ref.[145,146] (b) Atmospheric pressure radio-frequency (RF) torch-barrier discharge from ref.[43,44] (c) DBD with roll-to-roll deposition system on foils.[41,42] (d) Inductively coupled microplasma jet for localized treatments from ref.[45] (e) APP sustained by a direct current high voltage with precursor injection in the afterglow,[68,106,109] the blow arc by Axcys Technology is based on a very similar arrangement (see, e.g., ref.[81,82]) but excited by an alternate current (AC) instead of direct current (DC). Key distances which control the coating properties are "*d*" (nozzle-to-substrate) and "*δ*" (injector-to-nozzle, being either positive, the injector is located between the substrate and the nozzle, or negative, the injector is located before the nozzle). (f) The Atomflow RF-plasma reactor by Surfx Technologies.[47–50] (g) Generation of nanoparticles with hybrid plasma-liquid reactors.[52,53,58] (h) Plasma printing by atmospheric-pressure microplasmas for the patterned coating or surface modification of two- and three-dimensional substrates.[51] HV stands for high voltage and UHF for ultra-high frequency.

plasma. For review of the plasma printing technique, see ref.[51]

APPs can also be used for generation of variety of nanoparticles and nanostructures in a plasma-liquid synthesis process, where the plasma is facing the surface of a liquid and serves as a cathode in an electrolytic reaction (see Figure 2g). However, the plasma is not just the source of electrons for the reduction of metal ions, the chemical effects produced by the plasma–liquid interface system are far larger than those predicted by Faraday's law, which is explained by the fact that complicated chemical reactions induced by energetic ions (in the plasma) at the plasma–liquid interface are present in addition to charge transfer.[52,53]

The important factors of any plasma reactor operation are the energy consumption and gas flow needed for the treatment. APP can range from a very small energy consumptions in the range of few watt per cm^2 (e.g., DBD in filamentary mode and jets with noble gases) up to hundreds of watt per cm^2 in case of blown arcs or pseudo arcs (Figure 2e). This power consumption is comparable to low pressure plasmas. Also typical deposition rates, which range from a fraction of a nanometer per seconds to few hundreds of nanometers per seconds, are comparable with low-pressure plasmas. The biggest concern regarding the cost of operation of these plasmas is the typically very high gas flow,[19] which is, as already mentioned above, especially the issue for the plasma sources using noble gases as a plasma forming gas. Engineering solutions with capture and recirculation of this gas will be very probably needed in the future large area application to tackle this issue.

These challenges that are linked to APPs for material synthesis are the reasons why non-equilibrium APPs are not yet replacing well-established low-pressure plasma processes. On the other hand, the examples in this article document very clearly the future potential for APPs for the synthesis of variety of materials in new directions and new application requirements for next generation devices. Regardless, more experimental and theoretical works and engineering efforts are needed to exploit all the application potential of these APPs and to enable fast and large area treatment in industrial applications.

© 2016 The Authors. *Plasma Processes and Polymers* published by Wiley-VCH Verlag GmbH & Co. KGaA Weinheim
DOI: 10.1002/ppap.201500187

16128869, 2016, 1, Downloaded from https://onlinelibrary.wiley.com/doi/10.1002/ppap.201500187 by Technische Informationsbibliothek, Wiley Online Library on [24/01/2025]. See the Terms and Conditions (https://onlinelibrary.wiley.com/terms-and-conditions) on Wiley Online Library for rules of use; OA articles are governed by the applicable Creative Commons License

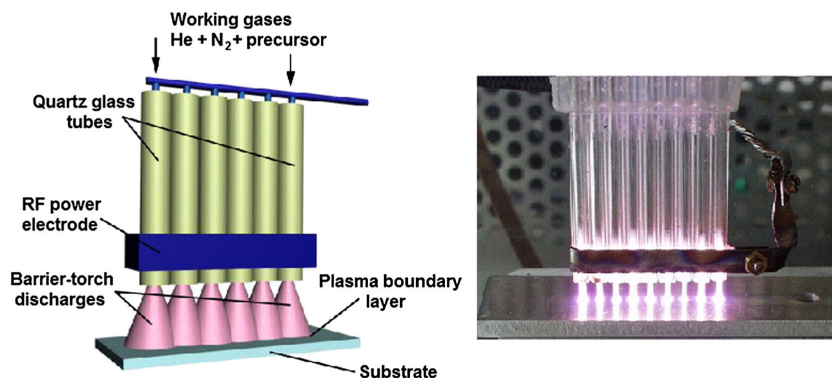

Figure 3. Array of a plasma jets for the homogeneous deposition/treatment of the substrate in one direction. Reprinted from ref.[78] Copyright (2009), with permission from Elsevier.

4. Photovoltaic Materials by Atmospheric Pressure Plasmas

4.1. Introduction

As previously discussed, APP reactors have been developed in a very wide range of configurations allowing for their use in very diverse applications. Therefore, one of the strongest features in APPs is their versatility in producing both a very wide range of materials as well as in very diverse modalities. Within the context of materials synthesis and processing for the fabrication of 3-Gen devices, APP processes can be classified in three different schemes for fabricating device components (Figure 5): (i) surface treatment; (ii) deposition; and (iii) nanomaterials synthesis followed by post-synthesis deposition.

Surface treatment by plasma processes can include passivation or modification of surface terminations as well as oxidation or localized heating (Figure 5a). Oxidation for instance can lead to both compact thin films but also to the growth of nanometric surface features. Materials synthesis and direct deposition (Figure 5b) relates to both thin films and the deposition of nanomaterials/nanoparticles to form nanostructured films and coatings. The first are generally represented by compact single- or large-crystal films where plasma-produced radicals reach the substrate unreacted. Nanostructured coating on the other hand are formed by the agglomeration of nanoparticles (NPs) nucleated and grown in-flight within the plasma before reaching the substrate. The third scheme (Figure 5c) involves the production and collection of NPs by various means, which can then be deposited on the application device by more standard techniques such as spin-coating, spray coating, etc. In the case of metal NPs, conductivity can be improved by annealing at reduced temperatures. It is clear that a combination of the three schemes is also possible so that for instance, composite materials with NPs embedded in bulk materials could in principle be produced. These different schemes of materials processing allows for APPs to be tailored to the different fabrication requirements.

While we will in general aim to demonstrate the possibility of a 3-Gen devices fully fabricated by APP processes (Figure 5d), it is clear that a successful device fabrication scheme will depend on many factors and therefore not all fabrication steps are expected to be implemented through APPs at a final manufacturing stage.

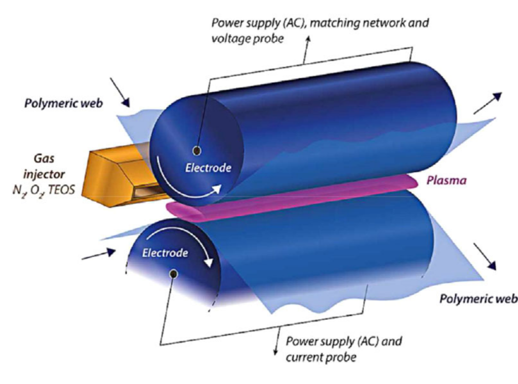

Figure 4. Experimental setup (left, reprinted with permission from ref.[42]) and photograph (right, credit to Marcel van de Kerkhof) of the process for deposition of high quality moisture barrier films on foils by an atmospheric pressure plasma in dielectric barrier configuration and excited by alternate current (AC) power. TEOS is tetraethyl orthosilicate.

4.2. Metal Contacts

Metal contacts should exhibit low resistance and adequate conductivity at the junction with the semiconductor or TBL. High vacuum systems are generally needed for fabricating these contacts through thermal evaporation, e-beam, or sputtering; however, APPs have demonstrated the possibility of producing suitable metal contacts (e.g., Cu, Au, Ag, Pd, etc.). Metal contact deposition can follow either a direct approach (Figure 5b) or a two-step process that involves first the synthesis and then the deposition of NPs (Figure 5c).

© 2016 The Authors. *Plasma Processes and Polymers* published by Wiley-VCH Verlag GmbH & Co. KGaA Weinheim

16128869, 2016, 1, Downloaded from https://onlinelibrary.wiley.com/doi/10.1002/ppap.201500187 by Technische Informationsbibliothek, Wiley Online Library on [24/01/2025]. See the Terms and Conditions (https://onlinelibrary.wiley.com/terms-and-conditions) on Wiley Online Library for rules of use; OA articles are governed by the applicable Creative Commons License

16128869, 2016, 1, Downloaded from https://onlinelibrary.wiley.com/doi/10.1002/ppap.201500187 by Technische Informationsbibliothek, Wiley Online Library on [24/01/2025]. See the Terms and Conditions (https://onlinelibrary.wiley.com/terms-and-conditions) on Wiley Online Library for rules of use; OA articles are governed by the applicable Creative Commons License

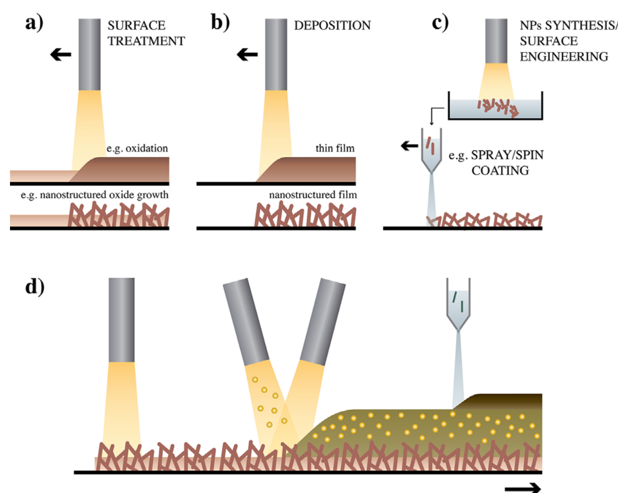

Figure 5. (a–c) Fabrication schemes by atmospheric pressure plasma (APP) of photovoltaic-relevant materials: (a) surface treatment such as oxidation leading, e.g., to oxide films or nanostructured oxides; (b) direct deposition of thin films or nanostructures to form films; (c) synthesis and collection of nanoparticles (NPs) for subsequent deposition via other techniques, or surface engineering or pre-synthesized NPs; (d) idealized full device fabrication of third generation devices by APP fabrication schemes.

4.2.1. Copper (Cu)

Copper can be an interesting choice for metal contact in PVs because of high conductivity and low cost. Utilizing a deposition scheme as shown in Figure 5b, nanostructured copper or agglomerate thin films can be deposited with a DC microplasma system with organometallic precursor, e.g., $Cu(hfac)_2$; the same process at different conditions can be used also for the deposition of different nanoscale film morphologies or for corresponding Pd and Ni films with $Pd(hfac)_2$ and nickelocene precursors, respectively. For instance under highly reducing conditions in N_2 background, dense Cu films can be produced with growth rates ranging from 0.3 to 4.5 nm s^{-1} (Figure 6).

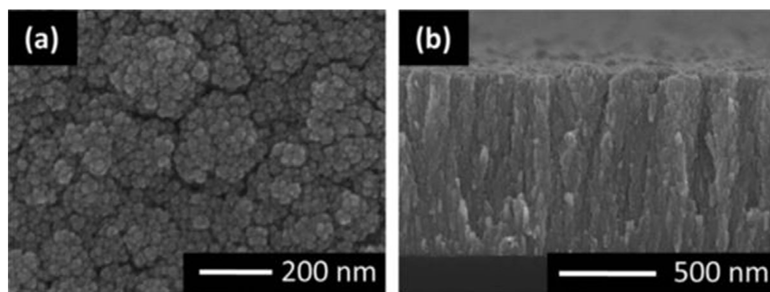

Figure 6. (a) Top–down and (b) cross-section views of Cu films deposited using a microplasma jet. Reprinted with permission from ref.[147] Copyright 2013, American Vacuum Society.

Lazea-Stoyanova et al. has also reported Cu NPs synthesis in gaseous environment directly by solid copper foil precursor.[54] A copper hollow RF-powered electrode and a ground stainless steel nozzle electrode were fitted in a cylindrical discharge chamber filled with argon at atmospheric pressure. The distance between the RF-powered electrode and the nozzle electrode was 27 mm and that between the nozzle and the substrate was 6 mm. RF power at 100 W was applied at the copper electrode to generate the plasma. Experiments were carried out with 1000 standard cubic centimeter (sccm) of argon flow through the hollow copper electrode and the product was deposited directly onto a silicon substrate. Metallic copper formation was confirmed by X-ray diffraction (XRD) and energy dispersive X-ray spectroscopy (EDX). Scanning electron microscopy (SEM) results revealed that vaporization of the copper electrode was responsible for Cu NPs formation by local melting. SEM and XRD results showed 100 nm diameter NPs. NPs, before deposition on the substrate, were well dispersed without agglomeration because in RF plasmas NPs become negatively charged and repel each other.[55]

Organometallic vapors can otherwise be used as a precursor to synthesize metal NPs.[56] Copper acetylacetonate $[Cu(acac)_2]$ salt was used as a precursor, vapors were generated by sublimation of solid $[Cu(acac)_2]$ at 383 K and introduced into a microplasma reactor with Ar gas flow at 100 sccm. A microplasma was generated between stainless-steel capillary tube and a stainless-steel mesh, sealed inside a quartz tube. DC power was applied at the electrodes keeping the current constant. The NP size distribution was obtained by in situ aerosol measurement. Analysis of these results showed that the NP synthesis rate increased by increasing precursor concentration. The effect of the discharge current on the NP size distribution was also explored. The mean diameter of the NPs was shifted from 4.0 to 3.5 nm as discharge current increased from 4 to 8 mA. This was explained as an effect of the gas temperature as this was increased by increasing current and high gas temperature led to more diffusion losses and reduced growth rate of particles because of the temperature-dependence nature of the Brownian diffusion coefficient.[57] The same approach could be used also for other metal NPs such as Ni, Fe, and Pt.

4.2.2. Gold (Au)

Gold is a very stable metal to corrosion with high conductivity. This is another metal which is used for making contacts in 3-Gen PVs due to the relatively high work function with respect to other metals. Gold metal production by APP

© 2016 The Authors. *Plasma Processes and Polymers* published by Wiley-VCH Verlag GmbH & Co. KGaA Weinheim
DOI: 10.1002/ppap.201500187

16128869, 2016, 1, Downloaded from https://onlinelibrary.wiley.com/doi/10.1002/ppap.201500187 by Technische Informationsbibliothek, Wiley Online Library on [24/01/2025]. See the Terms and Conditions (https://onlinelibrary.wiley.com/terms-and-conditions) on Wiley Online Library for rules of use; OA articles are governed by the applicable Creative Commons License

has been studied widely and has shown gold NPs production by different precursors. Patel et al.[58] has shown synthesis of gold metal NPs by APPs in contact with liquid without using any surfactant (similar to Figure 2g). This synthesis method would allow deposition of contacts following the fabrication scheme of Figure 5c. A carbon rod and stainless steel capillary was used as an anode and cathode, respectively. A high DC voltage up to 2 kV was applied at the anode while a stainless steel capillary cathode was grounded. Plasma was generated between the surface of gold (III)-chloride-trihydrate aqueous solution with concentration of 0.05–1 mM and stainless steel capillary, across 0.7 mm in the presence of 25 sccm helium gas flow. At lower precursor concentration (2.5 μM), all particles were spherical and less than 10 nm while higher concentrations (0.05–0.1 mM) solution produced a range of NP sizes and shapes. Discharge current effect on NPs synthesis was also monitored. Increasing the discharge current increased synthesis rate but did not change the particle size. These NPs were electrostatically stable without any surfactant. This synthesis and stable nature of NPs was explained on the basis of hydrogen peroxide formation in liquid by plasma processing. The same plasma-liquid approach could be used to produce Au NPs from a solid precursor (Au foil).[59] The microplasma setup included a Au foil anode and a stainless steel capillary cathode. The anode was immersed in an electrolyte (a dilute concentration of acid in deionized water) and placed 3 cm away from the cathode. The cathode was kept in close proximity of the solution at 1 to 2 mm distance and 25 sccm Ar gas was flown through the cathode. A DC voltage was used to ignite the plasma at the solution surface and maintained at a constant discharge current of 5 mA. The analysis of the samples was carried out with both ultraviolet-visble (UV-Vis) and transmission electron microscopy (TEM). It was shown by UV-Vis measurements that the NPs growth rate was faster using the liquid precursor, keeping other parameters constant. For the synthesis with a metal foil, a time lag was observed before NPs began growing, which could be due to the time required for metal cations to form and reach the microplasma–liquid interface. TEM results revealed mean particle size of ~10 nm.

4.2.3. Silver (Ag)

Chang et al.[60] showed APP synthesis of Ag NPs with an analogous process to the one described for Au NPs above (e.g., Figure 2g). Also in this case, contact deposition would follow Figure 5c scheme. A Pt metal foil anode was immersed in an aqueous electrolyte containing 1 mM $AgNO_3$ and a stainless steel capillary tube cathode was placed 3 cm away from anode and 1 mm above the solution. A negatively biased DC voltage of 290 V and 2 mA constant current was applied at the anode, which generated a plasma between the solution and the cathode in the presence of 25 sccm Ar gas flow. It was suggested that the gas phase electrons are responsible for reducing metal ions and nucleation.[61] The effect of process time on NPs synthesis was studied by UV-Vis absorbance. The UV-Vis spectrum showed that the synthesis rate was increasing over time but the size of the NPs did not change as there was no shift in the absorption peak position. Similar results were found for higher discharge currents,[59] which, however, led to particle agglomeration. Although a "clean" chemistry with no reducing agents and no surfactants is one of the benefits of this hybrid plasma-liquid approach, stabilizers can be used to improve control over NP properties. For instance, a common green stabilizer, fructose, was used to prevent uncontrolled growth and agglomeration of NPs.[62] The gap between the reaction volume and the stainless steel capillary was 2 mm. Helium was used as carrier gas and set to 25 sccm. A DC voltage of ~2 kV was applied on 10 mL of reaction volume with process time of 15 min and current of 3 mA to ignite the microplasma. The effect of the solution composition, temperature of electrolyte, presence of a stabilizer, and stirring of solution were studied. Effect of precursor concentration was similar as previously reported.[56] By increasing electrolyte temperature from 25 to 70 °C increased the synthesis rate and there was no effect of stabilizer on particle growth. Agitation of the solution increased the particle formation. The same principle of plasma-liquid synthesis was also demonstrated with AC plasmas.[63] A tungsten rod and a copper film were used as high voltage low voltage electrode. A solution, containing 0.2 g $AgNO_3$ precursor and 1.3 g poly vinyl pyrrolidone capping agent dissolved in 100 mL ethanol. Initially, 20 mL of this solution was taken to be treated by the plasma. A 5 kV high voltage power supply (500 W, 50–100 kHz, 0–30 kV, and working frequency 67.5 kHz) was applied and distance between tungsten electrode and ethanol solution surface was 3–5 mm. Argon gas was used as working gas with the flow rate of 0.3–1 L min^{-1}. A capacitor and a resistor were connected between the power supply and the plasma to limit the discharge current and to produce a stable glow discharge. The growth of NPs depends on the charge transferred during the discharge process. Smaller NPs sizes could be observed by applying shorter pulses,[64] which suggest AC current should be more effective than DC to control particle size. Small NPs (2–5 nm diameter) could be produced for instance using RF plasmas.[65,66]

4.3. Transport and Blocking Layers

Transport and blocking layers are mainly represented by wide bandgap oxides which have either p-type or n-type behavior. Oxides with the Fermi level close to the valence

© 2016 The Authors. Plasma Processes and Polymers published by Wiley-VCH Verlag GmbH & Co. KGaA Weinheim

16128869, 2016, 1, Downloaded from https://onlinelibrary.wiley.com/doi/10.1002/ppap.201500187 by Technische Informationsbibliothek, Wiley Online Library on [24/01/2025]. See the Terms and Conditions (https://onlinelibrary.wiley.com/terms-and-conditions) on Wiley Online Library for rules of use; OA articles are governed by the applicable Creative Commons License

band-edge (p-type) are generally used for hole-transport and electron-blocking layer, while oxides with the Fermi level close to the conduction band-edge are used to block holes and allow the transport of electrons. Intentional doping is not used for these layers as the formation of an internal electric field is required during device operation. Chemical synthesis of these oxides is by far the most used method, which generally produces nanostructures in colloids followed by spin- or spray-coating. Chemical synthesis is quite reliable but involves multiple and lengthy procedures, which do present limitations in terms of scalability and reproducibility. APPs can offer some advantages as they are capable of forming thin films directly on substrates (Figure 5a and b). The synthesis of oxide nanoparticles in-flight in gas phase is also possible with APPs, which provides great flexibility for direct deposition of nanostructured coatings (Figure 5b) or for collection in colloids followed by spin/spray coating (Figure 5c). Important materials for TBLs are ZnO, TiO_2, MoO_3, NiO, Cu_2O, CuO, etc. Metal contact deposition by APPs has found relatively minor interest than APP-based fabrication of oxides and therefore APP technologies for oxide growth/deposition are in many cases close to industrial feasibility. The reason for this is probably due to existing challenges and a strong demand for a range of metal oxides with tailored properties, while metal deposition have well-established technologies with very little opportunities for diversification or improvements. Oxides produced by APPs are summarized in Table 1.

4.3.1. Zinc Oxide (ZnO)

Direct deposition (Figure 5b) of un-doped ZnO assisted by APPs plasmas has been widely studied.[45,67] In most studies, substrates under the coating process are moved past the source to cover wide areas. In ref.,[67] the afterglow of a blown arc discharge in air (pulsed, 120 kHz alternate current at 600 W) between two coaxial electrodes was used to assist chemical vapor deposition. Zinc nitrate hexahydrate, used as precursor, was diluted in ethanol to produce an aerosol with N_2 as nebulizer gas. 135 nm thick ZnO films, consisting of agglomerates of nanometric particles, exhibited transparency below 80%, even after annealing with temperatures between 600 and 700 K. Hsu et al.[68,69] used a similar plasma arrangement (Figure 2a) but achieved much better results, probably thanks to a less powerful source which favors surface reactions versus gas phase synthesis of nanopowders. The discharge, which undergoes a glow-to-arc transition within each pulse power period, was fed by a direct current (DC) generator pulsed at 25 kHz. Zinc chloride diluted in water is used as the precursor whereas N_2 is used as carrier gas in the plasma jet. If sufficient time is left to the precursors in the afterglow, ZnO with transparency well above 80% and resistivity of $1.4\,\Omega\,cm^{-1}$ grows instead of zinc hydroxide chloride. The substrate temperature is below 673 K during the treatment. Penkov et al.[70] also employed a powerful blown arc discharge (DC plasmatron at $\sim$1 kW). Oxygen and a 5% ethanol solution of zinc acetylacetonate were successively introduced in the afterglow of the argon arc. Low temperature treatments could be achieved (393–423 K) by varying the deposition parameters but this also limited the deposition rate ($<1.5\,nm\,s^{-1}$).[71] The optical transmittance of the deposited amorphous ZnO films was around 90% in the visible region, despite trace copper due to electrode erosion. Although the layer resistivity could be improved by removing the top most carbon-contaminated layer, it remained very high ($3.0 \times 10^4\,\Omega\,cm^{-1}$). Annealing in hydrogen at 823 K could decrease the resistivity down to $5\,\Omega\,cm^{-1}$, which is still not sufficient for applications.

However, the high deposition temperature ($>$673 K) needed to achieve these results hinders the application of ZnO films to thermally sensitive materials, such as chalcogenide solar cells and plastic substrates for flexible solar cells. Lower deposition temperatures (473 K and even room temperature) were achieved, respectively, with a radio frequency (RF) atmospheric pressure plasma and the Atomflo 400D plasma source by Surfx Technologies.[72,73] Both processes used diethylzinc as precursor and helium as plasma gas, which, however, strongly limits their use at industrial scale. Oxygen is supplied in one case by introducing water in the plasma process whereas in the second case, oxygen is derived from air exposure after synthesis. The visible transmittance of these ZnO films is higher than 90%, however, the resistivity is also high and exhibits a wide variation. By a short post-deposition exposure to near-ultraviolet light, Illiberi et al.[72] could lower the resistivity to $1.6 \times 10^{-3}\,\Omega\,cm^{-1}$.

Resorting to metal-organic precursors, which are, however, generally expensive, can contribute to decrease deposition temperatures. Ito et al.[74] used bis(octane-2,4-dionato)zinc and could grow highly transparent ZnO coatings by APP at temperatures between 373 and 523 K. They obtained very high rates ($\sim$70 nm s^{-1}). Suzaki et al.[75] obtained similar features of ZnO films from bis(dipivaloylmethanato)zinc. They measured a minimum resistivity of $2.73 \times 10^{-3}\,\Omega\,cm^{-1}$.

Microplasmas were also tested in 2010.[45] A solenoid coil wound around a quartz capillary tube (1.1 mm inner diameter) in which a Zn wire (diameter 0.25 mm) is inserted excites an Ar plasma (delivered power $\sim$20–30 W and deposition rates $\sim$30 nm s^{-1}; Figure 2d). The Zn wire melts and emits a metallic vapor which reacts on the substrate located outside the capillary with oxygen coming from ambient air. Optical transmittance up to 90% in the visible was measured. Because of the very small size of the treated area, microplasmas would be an alternative to

© 2016 The Authors. *Plasma Processes and Polymers* published by Wiley-VCH Verlag GmbH & Co. KGaA Weinheim
DOI: 10.1002/ppap.201500187

Table 1. Summary of experimental conditions for the synthesis of various oxides by atmospheric pressure plasma (d and δ are defined in Figure 1).

Source	Conditions	Thin film	Plasma gases	Precursors	T (°C)	v_d [nm min^{-1}]	Distances [mm]	Speed scan	Ref.
APPJ (post-treatment)	DC pulse @ 25 kHz (275 V) Duty cycle: 17.5%	TiO_2	N_2: 31 sLm		500		$d = 27$	0.5 mm s^{-1}	[79]
Surface DBD	AC: 4.4 kV @ 15 kHz 0.6 W cm^{-2}	TiO_2	Ar: 900 sccm	$TiCl_4$ + 14 sccm Ar O_2: 9 sccm (through plasma)		22		–	[77]
APPJ	DC pulse @ 25 kHz (275 V) Transformer to 15 kV Duty cycle: 17.5%	ZnO	N_2: 45 sLm	$ZnCl_2$: 3 wt% in H_2O N_2 carrier gas: 500 sccm		77	$d = 25$	10 mm s^{-1}	[68]
Blown arc	AC pulse @ 100 kHz 600 W	TiO_2	N_2: 30 sLm	TTIP: 5 μL min^{-1} N_2 carrier gas: 5 sLm	190		$\delta = 25$ $d = 30$	3 mm s^{-1}	[81]
RF plasma	13.56 MHz RF plasma 60 W	ZnO	Water + He	Diethylzinc + He (through plasma)	200	420		0.3–1 mm s^{-1}	[72]
Plasma jet	Bipolar impulse voltage Amplitude: 6 kV @ 5–30 kHz	ZnO	He: 1 sLm	Bis(octane-2,4-dionato)zinc + 2 sLm He	100–250	4800	$\delta = 5$ $d = 10$	0.17 mm s^{-1}	[74]
Atomflo 250D	13.56 MHz RF plasma 80 W	ZnO	He: 20 sLm O_2: 75 sccm	$Zn(hfa)_2$(N,N′-DEA) + 3 sLm He $Al(tmhd)_3$ + 0.23 sLm He H_2O + 50 sccm He	<250		$d = 3$		[48]
BTD	13.56 MHz RF pulse @ 20–40 Hz 600 W	TiO_2	He: 150 sccm	Ti(O-i-Pr)$_2$(thd)$_2$ 355 sccm He + 110 sccm N_2		12	$d = 10$		[78]
DBD	Spacing: 2.2 mm	SnO_2	N_2 or air	Tetrabutyltin or monobutyltin trichloride (through plasma)	80	150	$d = 2–6$		[98]
Atomflo 250D	13.56 MHz RF plasma 110 W	In_2O_3	Helium O_2: 200–500 sccm	In(acac)3 + 5.5 sLm	<250		$d = 2$	14 mm s^{-1} Pitch: 2 mm	[49]

© 2016 The Authors. *Plasma Processes and Polymers* published by Wiley-VCH Verlag GmbH & Co. KGaA Weinheim

16128869, 2016, 1, Downloaded from https://onlinelibrary.wiley.com/doi/10.1002/ppap.201500187 by Technische Informationsbibliothek, Wiley Online Library on [24/01/2025]. See the Terms and Conditions (https://onlinelibrary.wiley.com/terms-and-conditions) on Wiley Online Library for rules of use; OA articles are governed by the applicable Creative Commons License

16128869, 2016, 1, Downloaded from https://onlinelibrary.wiley.com/doi/10.1002/ppap.201500187 by Technische Informationsbibliothek, Wiley Online Library on [24/01/2025]. See the Terms and Conditions (https://onlinelibrary.wiley.com/terms-and-conditions) on Wiley Online Library for rules of use; OA articles are governed by the applicable Creative Commons License

conventional fabrication techniques for localized, high-rate deposition of functional ZnO films.

4.3.2. Titanium Di-Oxide (TiO_2)

TiO_2 is widely used for solar cells, especially in the anatase phase. Deposition of nanoporous films at low temperature are of great interest for solar cells. Coplanar[76] and surface[77] dielectric barrier discharge (DBD; excited by a bipolar sine wave with 4.4 kV peak-to-peak voltage at a frequency of 15 kHz) were used for APP chemical vapor deposition (CVD) of TiO_2 films from $TiCl_4$ and O_2, both carried by argon. A maximum growth rate of 0.37 nm s^{-1} could be achieved. As amorphous films were obtained, calcination in air at 623 K was needed to form anatase.

Kment et al.[78] designed a new plasma reactor, named the atmospheric pressure barrier torch discharge (BTD; Figure 2c), to circumvent the main limitation of standard DBD system, which is the treatment of only flat and well-accessible surfaces. The BTD is produced by an RF generator with only one electrode in the system. With such a source, these authors deposited TiO_2 thin films from a solid precursor $Ti(O\text{-}i\text{-}Pr)_2(thd)_2$ (Titanium(IV) diisopropoxide bis(2,2,6,6-tetramethyl-3,5-heptanedionate)) placed in an evaporation cell at 405 K and transported by a mixture He-N_2 in the discharge. Much lower flow rates were also used compared to those usually employed, i.e., hundreds of sccm versus tens of liters per minute (sLm). TiO_2 thin films were made of different phases (amorphous, anatase, rutile, brookite) depending on the conditions and deposited close to 420 K at rates inferior to 0.2 nm s^{-1}.

Chang et al.[79] sintered a 10 μm-thick paste of TiO_2 screen-printed on fluorine-doped tin oxide glass by applying a nitrogen APP. The same method was applied by Yuji et al.[80] with almost the same source (non-equilibrium Ar-N_2 plasma fed by a DC pulse power supply: 10.0 kHz at 150 W). Typically, the treatment temperature is about 773 K[79] and permits to get ~80% of anatase in the nanoporous TiO_2. The plasma treatment is much shorter than calcination[79] but leads basically to the same results; no significant difference in the surface state stoichiometry was observed among furnace-sintered and APP-sintered TiO_2 layers.[79] On the basis of this latter observation, the role of surface chemical reactions, which lead to grafting and nitriding of the TiO_2 surface according to ref.[80] needs to be clarified.

Maurau et al.[81] used a nitrogen atmospheric pressure blown arc developed by Axcys Technology (Figure 2e) to deposit photo-active coatings at 460 K from titanium tetraisopropoxide (TTIP) injected after the nozzle exit, in the remote area of the discharge. The process forms nanoparticles in the gas-phase which are then agglomerated at the substrate producing a nanostructured film as proposed in scheme of Figure 5b. The nanoparticles were crystalline and contributed to a strong increase in the specific area of the coating. The same group[82] also used titanium bis(acetylacetonate)diisopropoxide (TIPO) as precursor with the same arrangement. This compound is far less sensitive to water than TTIP, making it a bit easier to handle. Deposition temperatures were slightly higher (488 K) but led to films with similar structures to those found with TTIP (Figure 7d).

4.3.3. Molybdenum Oxide ($MoO_{2/3}$)

Shrotriya et al. replaced successfully PEDOT:PSS by MoO_3[83] and V_2O_5[84] as hole selective layer. The thickness of the MoO_3 layer is a key parameter in the efficiency of inverted solar cell structures. Wang et al.[85] showed that the probability of bimolecular recombination either at the interface with the anode or within the active layer itself is minimized for nanometric layers (~10–20 nm typically), given high values of the short-circuit current density. Then, the MoO_3 layer is an effective hole-transporting, electron- and exciton-blocking layer.

At atmospheric pressure, several processes were proposed to synthesize molybdenum oxides.[86–93] Lebid

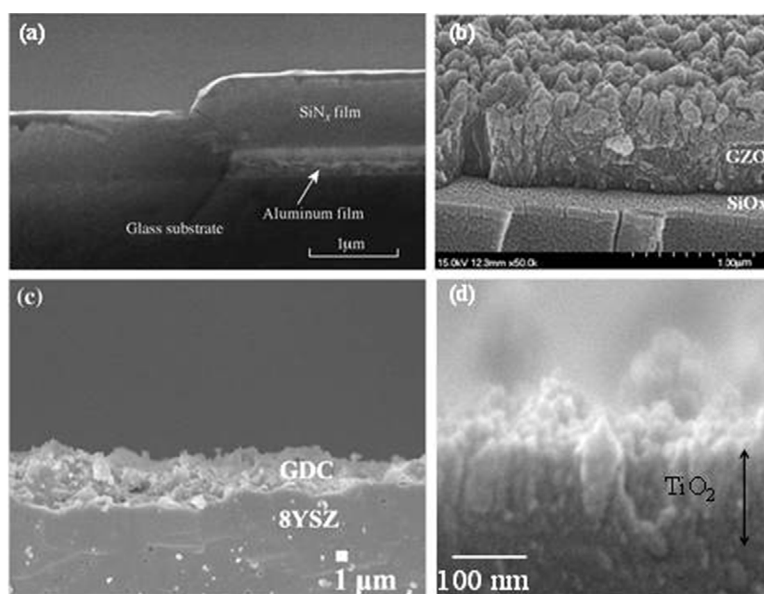

Figure 7. Examples of deposited thin films. (a) SiNx deposited by rotary dielectric barrier discharge; reprinted from ref.[125] Copyright (2005), with permission from Elsevier. (b) Gallium-doped ZnO deposited by atmospheric pressure plasma (APP); reprinted from ref.[107] Copyright (2013), with permission from Elsevier. (c) Gd_2O_3-doped ceria deposited by APP; reprinted from ref.[102] Copyright (2014), with permission from Elsevier. d) TiO_2 deposited by blow arc, see ref.[39] for experimental conditions.

© 2016 The Authors. *Plasma Processes and Polymers* published by Wiley-VCH Verlag GmbH & Co. KGaA Weinheim
DOI: 10.1002/ppap.201500187

16128869, 2016, 1, Downloaded from https://onlinelibrary.wiley.com/doi/10.1002/ppap.201500187 by Technische Informationsbibliothek, Wiley Online Library on [24/01/2025]. See the Terms and Conditions (https://onlinelibrary.wiley.com/terms-and-conditions) on Wiley Online Library for rules of use; OA articles are governed by the applicable Creative Commons License

et al.[86] elaborated orthorhombic α-MoO_3 millimetric crystals by electric arcs in air between metallic molybdenum electrodes. The atmospheric microplasma process described in ref.[87–93] is best suited to deposit thin films. The process can either be direct (Figure 5b) or used to synthesize colloids which can be deposited next by spin- or spray-coating (Figure 5c). Moreover, the use of atmospheric microplasma introduces several benefits such as reduced implementation costs, atmospheric working pressure, non-equilibrium and low processing temperature, and a characteristic microplasma chemistry which would be unattainable with larger scale plasmas.[94]

Bose et al.[87] used a microplasma system based on a molybdenum wire (100 μm in diameter) placed in a sub-millimetric capillary ($\sim$700 μm) around which a 20-turn Cu coil was wound. The coil was connected to an ultra-high frequency (450 MHz) power supply via a matching circuit, while the other end was left floating. The discharge was ignited in an Ar-2% O_2 gas mixture. The stable generation of microplasma inside the quartz tube led to spraying of the nanoparticles onto a silicon substrate placed 200 μm away from the nozzle exit. Mariotti et al.[88–91] used almost the same device but, rather than using a coil, these authors connected the patch molybdenum antenna (100 μm in diameter) directly to the ultrahigh frequency (450 MHz) power supply. With such a configuration, they could not only grow different nanostructures and nanoarchitectures with regards to Bose's configuration, but also produce self-organized nanostructures on the substrates, thanks to the propagation of the ultra-high frequency field up to the substrate. Basically, the wire is consumed after ignition because of the wire oxidation and followed by evaporation of molybdenum oxides which have a much lower melting temperature (1373 K for MoO_2 and 1068 K for MoO_3) than molybdenum (2896 K). With the microplasma system, depending on the conditions, various oxides, nanostructures and nanoarchitectures could be obtained, from MoO_2 nanoparticles to monoclinic β-MoO_3 nanosheets. Although the microplasma-based process is in principle scalable to process large-area surfaces cost-effectively and reliably, it remains more directly adapted to local treatments.

More recently, Pai et al.[92,93] showed that nanosecond repetitive pulsed discharges, because they achieve high energy efficiency, enhance plasma-chemical processes that are useful for synthesis. These discharges enable fast heating and cooling, which may be responsible for the formation of non-equilibrium material phases. Using a corona-like arrangement, Pai et al.[93] applied short (40 ns) high-voltage (12.5 kV) pulses at 30 kHz across molybdenum electrodes in open ambient air, generating a nanosecond spark discharge that synthesized well-defined MoO_3 nanoscale architectures like flakes, dots, walls, and porous networks. Because of the low-average temperature, deposition on labile substrates like polymers was possible. The presence of α-MoO_3 is explained by the existence of huge thermal gradients that would lead to surface temperatures above 723 K while keeping cool the polymer bulk.

Depositing molybdenum oxides with adapted properties by APPs for photovoltaics seems possible leading to large specific surface areas obtained with nanostructures. Direct evaporation of molybdenum oxides from a wire might also give denser continuous layers, but another strategy, based on a gaseous precursor seems also appropriate to explore.

4.3.4. Copper (CuO/Cu_2O), Palladium (PdO), and Nickel Oxides (NiO)

Similarly to Mo-oxides, Ni-/Cu-oxides are important p-type TBLs that add flexibility in designing device architectures. A range of CuO and NiO thin film morphologies can be deposited through direct deposition (Figure 5b) from $Cu(hfac)_2$ and $Ni(hfac)_2$ in oxygen-based DC microplasmas.[95,96] Growth rates were evaluated to be $\sim$70 and $\sim$400 nm min^{-1} for NiO and CuO, respectively. The same process can be applied with $Pd(hfac)_2$ leading to PdO films with growth rates of $\sim$25 nm min^{-1}.[95] It should be noted that bulk CuO has a nominal bandgap of $\sim$1.2 eV and therefore it is potentially a suitable absorber, however, experimentally measured optical bandgap reports values of 1.8–1.9 eV indicating possible quantum confinement effects originating from the film nanocrystallinity and consequent widening of the bandgap. Direct deposition of Cu_2O has proven to be more difficult due to its propensity to oxidize; some progress is being made in the synthesis of Cu_2O NPs with hybrid plasma-liquid approaches, which would then allow post-synthesis deposition by spray/spin-coating techniques (Figure 5c).

4.3.5. More on TBLs

The atmospheric pressure BTD system has already been successfully applied for the low-temperature coatings of In_2O_3,[43,49] SnO_x,[43,97–99] ITO,[100] CeO_x,[44,101] and CeO_x doped by Gd_2O_3[102] (Figure 2c). This and other experimentation have clearly demonstrated APP capability to cover the wide range of TBL materials and to deal with solid, liquid, and gaseous precursors. There is no doubt that research in APPs will bring TBL coatings and nanostructured films with suitable and competitive properties for application in 3-Gen PV devices. The ideal APP process should avoid the need of subsequent annealing step and deposition rates should also be improved.

4.4. Transparent Conductive Contacts

When III A elements like In^{3+}, Ga^{3+}, and Al^{3+} are used as dopant at concentrations as high as 10^{21} cm^{-3} on

© 2016 The Authors. *Plasma Processes and Polymers* published by Wiley-VCH Verlag GmbH & Co. KGaA Weinheim

16128869, 2016, 1, Downloaded from https://onlinelibrary.wiley.com/doi/10.1002/ppap.201500187 by Technische Informationsbibliothek, Wiley Online Library on [24/01/2025]. See the Terms and Conditions (https://onlinelibrary.wiley.com/terms-and-conditions) on Wiley Online Library for rules of use; OA articles are governed by the applicable Creative Commons License

Zn^{2+} lattice sites in ZnO, they promote metal-like electrical properties but reduce carrier mobility owing to neutral and ionized impurity scattering.[103] Low resistivity ($\sim 10^{-4}\,\Omega\,cm^{-1}$) and good optical properties (transparency in the visible region >90%, optical index n ∼2), makes doped ZnO an excellent candidate as a TCO in solar cells. However, TCO films are very sensitive to defects. Then, the control of the film composition and structure over its whole thickness is essential. APPs do not benefit from energetic ions and constrains on deposition temperatures limit the quality of the films. The choice of the plasma source for plasma-enhanced chemical vapor deposition (PECVD) is then a key parameter for given precursors.

Among TCO coatings, zinc oxide is used in 2-Gen solar cells with absorber layers based upon semiconducting $CuInSe_2$ and $Cu(In,Ga)Se_2$. A ZnO double layer is typically employed. An inner intrinsic sublayer with higher resistivity acts as a shunt barrier. An outer aluminum-doped ZnO (AZO) layer collects the photo-generated charge carriers.[104] Besides lateral electrical conduction, heavily doped AZO moves the space charge region deeper into the p-type semiconductor layer, which improves the internal quantum efficiency of the device.[105] AZO layers were first deposited at 498 K by plasma-enhanced chemical vapor deposition at atmospheric pressure in 2007.[47] An Atomflo-250D device from Surfx Technologies (Figure 2b) was run at 75 W for deposition. A film resistivity of $3.3 \times 10^{-2}\,\Omega\,cm^{-1}$ (aluminum concentration $5.4 \times 10^{20}\,cm^{-3}$) and a transparency of 95% from 375 to 2500 nm was obtained for a deposition rate of $1.2\,nm\,s^{-1}$. An rf-driven He-1.25‰ CO_2 DBD afterglow with a grid electrode was fed with diethylzinc (25 ppm) and trimethylaluminum (0.25 ppm).

The same plasma system was used at 80 W by Johnson et al.[48] in 2013 for the same purpose but with different precursors. These authors found out that the six-coordinate metal-organic complex $Zn(hfa)_2$(N,N′-DEA) exhibited superior transport characteristics as compared to four-coordinate $Zn(acac)_2$ and $Zn(tmhd)_2$ metal-organics. The non-fluorinated metal-organic precursor $Al(tmhd)_3$ was used in conjunction with $Zn(hfa)_2$(N,N′-DEA) to give AZO at 573 K. The addition of water vapor in the plasma reduced the amount of ligand-derived fluorine contamination to less than 1 at%. This led to AZO films with minimum resistivity of $1.1\,\Omega\,cm^{-1}$ with a growth rate of $0.042\,nm\,s^{-1}$. It turns out that the lack of grain boundaries in the amorphous phases grown at low process temperatures (below typically 500 K), as in the work of Barankin et al.,[47] improves the electrical resistivity of the films. The columnar growth of small circular grains at high temperature (above typically 550 K) generates boundaries full of defects which alter the electrical conductivity.

Chang et al.[106,107] used a plasma jet generated by applying a DC power pulsed at 20 kHz (named APPJ for atmospheric pressure plasma jet), Figure 2a. Gallium-doped ZnO (GZO) films were deposited on SiO_x-coated glass at 150 °C using $Zn(NO_3)_2$ and $Ga(NO_3)_3$ as precursors (Figure 7b). A minimum resistivity of $6 \times 10^{-4}\,\Omega\,cm^{-1}$, corresponding to a carrier concentration of 6.58×10^{20} cm^{-3}, is achieved at 8 at% gallium doping. The maximum transparency in the visible region reaches about 80%. The enhancement in crystallinity increases both carrier mobility and carrier concentration and results in a decrease of resistivity, a drastically opposite behavior to AZO. Also, these authors showed the influence of the texture of the SiO_x sub-layer on the haze value of the stack GZO/ SiO_x in the visible and near-infrared regions, rougher surfaces contributing to increase the haze.[108] Then, APPJ is an effective method for preparing textured TCO.

Indium-doped ZnO (IZO) films were deposited by Chang et al.[109] with the same DC-pulsed APPJ as in ref.[106,107] Zinc nitrate and indium nitrate were used as precursors and dissolved in water in desired amounts. The solution was ultrasonically atomized and then conveyed by nitrogen to the plasma, also sustained in nitrogen. The power, set at 600 W, led to a substrate temperature of 473 K. The IZO surface morphology is affected by indium doping, so that needles shape the surface from 6 to 10 at% In. The indium would lie distributed randomly on the ZnO film, thus preventing an orderly arrangement. 8 at% indium-doped zinc oxide films show a low resistivity of $1.8 \times 10^{-3}\,\Omega\,cm^{-1}$, corresponding to a carrier concentration of 2.69×10^{20} cm^{-3}, the transmittance being about 80% in the visible range. The grain size is about 25 nm. Then, the IZO films exhibit very similar features to GZO films deposited by the same group.[106,107]

4.5. Active Layer Materials

The active layer of the general device structure in Figure 4 is formed either by inorganic quantum dots only or together with a matching material to form a hetero-junction or a bulk hetero-junction. Matching materials used in 3-Gen PV devices have been so far represented by semiconducting polymers such as P3HT, PTB7, etc. These hybrid inorganic–organic active layers have generally relied on standard solution processing to deposit the polymer/QDs composites. The synthesis of semiconducting polymers by APPs is certainly a possibility; however, at this time, there has been no attempt to produce a full hybrid active layer using solely APPs. This is probably because, while APP may be capable of producing the whole polymer-QDs composite, it may be difficult to compete with solution processing for this type of devices. Therefore, plasma processing at atmospheric pressure has been so far limited to the modification of the surface characteristics of QDs and to improve the interface interactions with the polymer matrix (see further below). The active layer can be formed also with an inorganic matching material.

© 2016 The Authors. Plasma Processes and Polymers published by Wiley-VCH Verlag GmbH & Co. KGaA Weinheim
DOI: 10.1002/ppap.201500187

However, very few examples of all-inorganic active layers have been reported in the literature; these are junctions formed between inorganic QDs and another inorganic material, which could be also represented by a different type of QDs.

Third generation devices have mainly employed PbSe, PbS, PbTe, CdSe, Si, and Ge QDs.[110–112] Wet chemical synthesis is by far the preferred method for most of these QDs, with also best devices efficiencies reaching ~7%.[112] Plasmas, in particular low-pressure plasmas, have, however, demonstrated superior results in the synthesis and device integration of Si and Ge QDs, also referred to as Si-/Ge NCs. Low-temperature plasma technologies have focused on the synthesis of Group IV materials mainly because plasma environments offer highly suitable conditions to deal with high melting temperature materials such as silicon. In principle, plasmas could be used to synthesize Pb- and Cd-based QDs, however, the exceptional results achieved by wet chemical methods is undermining the motivations for initiating at this stage research activities in plasma synthesis for these types of materials. Furthermore, the toxicity of lead and cadmium represents a non-trivial obstacle for the integration of these QDs in application devices. Metal sulphides nanocrystals offer for instance much more promising and "green" avenues for plasma synthesis research.[113] As research in APPs is catching up with the "older" low pressure plasma technologies, great opportunity exist for APP QDs synthesis. Nonetheless, Si NCs are essentially the only type of QDs for active layers in 3Gen PVs that have been synthesized by APP.

Atmospheric pressure microplasmas are very versatile tools to control the composition and crystallinity of Si-based QDs.[114,115] Nucleation, growth, and nanoparticle heating are mechanisms closely related in APPs. Although further confirmation will be required, nucleation in APPs appears to take place via supersaturation of silicon atoms rather than through a polymerization process of SiH_x radicals as observed in low-pressure plasmas; this is partly supported by strong emission of atomic silicon lines in silane-based APPs.[115,116] Therefore full silane dissociation is necessary in APPs to achieve crystalline Si QDs. Nanoparticle heating in APPs is analogous to low-pressure plasmas, however, an increased collisionality regime should be taken into account, which generally leads to higher nanoparticle temperatures for a wider range of plasma parameters.[117] It should be noted that even if the plasma conditions allow for nanoparticle to reach the required crystallization temperature, these might be still amorphous (e.g., a-Si:H QDs[15]) if full silane dissociation is not initially promoted.

The synthesis of Si NCs by APPs was reported over the past decade.[114–116] Our recent work has shown that device-grade Si NCs can be produced by APPs.[114–117] This progress has also shown the possibility of producing Si NCs in quantities that are suitable for research-grade PV device fabrication (see further below). The most recent developments use enlargeable microplasma systems sustained by 13.56 MHz power (see Figure 8).[114]

In this case, silane is used as precursor mixed with argon and hydrogen at various concentrations.[114] Electrodes, made of copper, are positioned at both sides of a quartz capillary with a rectangular cross section ($0.5 \times 5\,mm^2$ internal and 0.3 mm wall thickness). The electrodes are 20 mm long in the quartz tube axial direction and 5 mm thick covering the full thickness of the capillary (Figure 8). The plasma reactor is housed in a nitrogen-filled sealed stainless steel chamber in which the pressure is maintained at one atmosphere. Figure 8a and b reports two photos of this microplasma system, which also display the frame made out of Perspex holding all the components together. The schematic of Figure 8c depict the deposition of Si NCs on a ITO-patterned glass substrate which is then used for the fabrication of 3-Gen devices (see further below). Si NCs with size varying within 2–4 nm can be easily produced at $1.2 \times 10^{-13}\,kg\,h^{-1}\,m^{-2}$,[114] which is sufficient to produce research devices with ease.

APPs have been very little explored for the synthesis of active layer materials, including QDs. Recent progress achieved with the synthesis of Si NCs by APPs is very promising and it should stimulate further work covering a much wider range of materials for both QDs as well as matching materials. While organic-, Pb-, and Cd-based materials might not offer long-term opportunities for APP processes, environmentally friendly metal-sulphides,

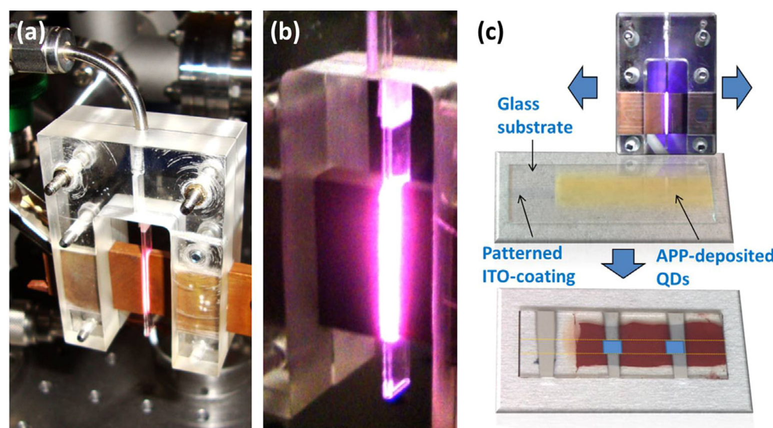

Figure 8. (a and b) Photos of an atmospheric pressure plasma (APP), specifically a microplasma system, used for the synthesis of silicon quantum dots (QDs). (c) Schematic depicting the deposition of silicon QDs on a glass substrate with a patterned indium tin-oxide (ITO) coating (reprinted and adapted with permission from ref.[114]).

© 2016 The Authors. *Plasma Processes and Polymers* published by Wiley-VCH Verlag GmbH & Co. KGaA Weinheim

16128869, 2016, 1, Downloaded from https://onlinelibrary.wiley.com/doi/10.1002/ppap.201500187 by Technische Informationsbibliothek, Wiley Online Library on [24/01/2025]. See the Terms and Conditions (https://onlinelibrary.wiley.com/terms-and-conditions) on Wiley Online Library for rules of use; OA articles are governed by the applicable Creative Commons License

16128869, 2016, 1, Downloaded from https://onlinelibrary.wiley.com/doi/10.1002/ppap.201500187 by Technische Informationsbibliothek, Wiley Online Library on [24/01/2025]. See the Terms and Conditions (https://onlinelibrary.wiley.com/terms-and-conditions) on Wiley Online Library for rules of use; OA articles are governed by the applicable Creative Commons License

alloys, and other composites can represent exciting new developments. APP direct deposition of a composite active layer (e.g., middle of Figure 5d) is also an important aspect where atmospheric pressure operation could bring specific benefits to reduce manufacturing costs.

4.6. Relevant Atmospheric Pressure Plasma Processes for Antireflection Coatings

Finally, it is worth mentioning that annealing post-treatments with different APPs of thin films deposited by other processes (e.g., Figure 5a) can be successfully used to enhance the shielding of ambient oxygen, defect and surface states passivation, and to promote highly conductive interfaces.[24–27] The nitrogen plasma-treated capping layers may at the same time increase the photocurrents and decay fast-saturation time constant. It is believed that the low conductivity passivation layer shields the ambient oxygen molecules and obstructs the charge relaxation process, leading to an increase in decay fast-saturation time constant.[24] When hydrogen is added to nitrogen in the plasma, only minor changes are observed.[26] However, when air is added downstream, the treatment temperature decreases. In the case of ITO coatings, the resistivity varies accordingly from 1.81×10^{-2} to $8.58 \times 10^{-4}\,\Omega\,cm^{-1}$ after 15 s of treatment owing to crystallization and oxidation processes that reduce the defect density in the material. Subsequently, the resistivity increases slightly to $1.71 \times 10^{-3}\,\Omega\,cm^{-1}$ after 90 s because of the reaction of oxygen that reduces the oxygen vacancies.[27]

Surface passivation of silicon solar cells can be efficiently achieved by plasma-enhanced chemical vapor deposition of silicon nitride films fabricated below 400 °C.[118–122] In addition to the favorable electronic properties, amorphous SiN_x:H films also act as a very effective antireflection coating on silicon.[118] SiN_x:H thin films deposited by plasma-enhanced chemical vapor deposition[123,124] contain about 8% to approximately 30% (atom) hydrogen. The hydrogen atoms diffuse to the SiN_x:H/Si interface and to the bulk of the sample, reducing the recombination activity of the impurities present in the material, thus performing volume passivation and improving the bulk carrier lifetime. These films have already been synthesized successfully by plasma at atmospheric pressure.[125–128] Kakiuchi et al.[125] used a very specific plasma system made of a high-speed (3000 rpm) rotary electrode fed by a 150 MHz power supply. The substrate, located less than 1 mm from the rotary electrode, can be heated up to 823 K. Enormous gas consumption (~1200 sLm) is used in these processes with N_2/NH_3 (1%), H_2 (1%), SiH_4 (0.05%), and He (balance), which is counterbalanced by very high deposition rates (up to 120 nm s^{-1}). These authors observed that the large difference in the dissociation energy of SiH_4 and N_2 molecules prevented the growth of homogeneous SiN_x:H films. This issue was addressed by using NH_3, which led to homogeneous and smooth films of SiN_x:H (Figure 7a) with N/Si atomic ratio varying from 1.28 to 1.18. Then, the refractive index could be adjusted between 1.69 and 1.81. SiN_x film with a dense Si-N network can be deposited if the power and the H_2 concentration are high enough. Indeed, at high power, highly dissociated precursors are produced, resulting in the introduction of a large amount of dangling bonds into the film. These bonds can be saturated by using high H_2 concentrations in the plasma, because hydrogen radicals efficiently terminate dangling bonds. They also remove the bonded H atoms on the surface to increase Si—N bonds. Then, by controlling the power and the hydrogen concentration, the sought quantity of H in SiN_x:H can be controlled. A DBD system was developed where a laminar gas flux is introduced between two barrel electrodes.[127,128] The plasma is fed at different frequencies ranging from low-frequency to RF (50 kHz to 7.3 MHz). Argon flowing at 6 sLm is used as carrier gas. NH_3 and SiH_4, in variable proportions, are introduced in such way that the partial pressure of the two gases is 200 part per million (ppm). Gas recirculation, favoring the synthesis of NPs and their further incorporation in the coating, must be crucially suppressed in this case. If a square-wave modulation at 200 Hz was applied, better passivation is achieved. By getting a refractive index of 2.1 and negligible absorption, minority carrier lifetime of 1 ms after rapid thermal annealing, APP grown SiN_x:H films exhibited the same performance as standard low pressure PECVD SiN_x:H.

Nowling et al.[50] used the Atomflow device (Figure 2f) to deposit SiN_x thin films. Although the deposition rate is insensitive to temperature, this variable does not only affect the film composition but also the hydrogen content. Firstly, less impurity (in carbon, oxygen, etc.) is found at higher deposition temperature. Secondly, at 373 K, the film has a total hydrogen content of 37.5 at% with 90% of the H atoms bonded to nitrogen. At 773 K, the total hydrogen content is reduced to 13.9 at% with 65% of the H atoms bonded to nitrogen. With low-pressure N_2/SiH_4 systems, the majority of hydrogen is bonded to silicon and most often, there is no detectable N—H bonding. Decreasing the temperature, or increasing the N_2/SiH_4 ratio, causes the hydrogen to be bonded almost exclusively to nitrogen. The dominance of N—H bonding is more characteristic of films produced in reactors using ammonia and silane reagents. The primary source of the hydrogen impurity being NH_3, high substrate temperatures are essential for minimizing the density of N—H bonds.

Hopfe et al.[129,130] developed two plasma sources operating at atmospheric pressure to coat large substrates. By resorting either to microwave excitation or a linear extended DC arc system, they could deposit silicon nitride as anti-reflectance coatings on silicon solar wafers with a similar quality as low-pressure PECVD thin films. Any

© 2016 The Authors. *Plasma Processes and Polymers* published by Wiley-VCH Verlag GmbH & Co. KGaA Weinheim
DOI: 10.1002/ppap.201500187

remote plasma configuration was considered better suited for continuous processing because the plasma chemistry cannot influence the source operation which is imperative to achieve long-term stability.[85,131] In high-power sources, gas temperature increases and gas hydrodynamic becomes extremely important to mix active species from the plasma with precursors. Particularly, transient phenomena become important and the correlated time evolution of the gas and surface temperatures may strongly influence the process yield.[132] In the case of the linear extended DC arc system, Hopfe et al.[129] preferred tetramethylsilane to silane and NH_3 to N_2, ammonia leading to dense, particle-free SiN_x:H thin films. No fundamental differences have been found between the two plasma activation methods.

4.7. Surface Engineering and Interfacial Processing to Improve Dissociation and Transport

The surface properties of NPs play a key role in determining corresponding NPs properties. Therefore surface treatment of NPs in colloids is an important process that can contribute to improve the integration of NPs in devices through methodologies as depicted in Figure 5c. Furthermore, control over interface properties are of paramount importance for carrier transport where defects can act as trap states and therefore largely deteriorate the collection efficiency. Surface passivation that maintains desired opto-electronic properties are therefore highly demanded, however, very limited work has been progressed in this sense with APPs.

As previously suggested, the device structure and the specific 3-Gen concepts can also improve carrier collection; therefore suitable approaches to interface engineering largely depend on the overall device architecture. For instance the incorporation of NPs into polymer matrices is very promising to improve the properties of hybrid organic–inorganic active layers.[133] A common problem associated with NPs is that they often tend to agglomerate in polymer because of surface incompatibilities resulting in substantial degradation of the active layer.[134] Various surface functionalization have been possible by dispersing both pre-synthesized Si NCs into water, ethanol, or other solutions and subsequently exposed to DC or RF microplasmas;[135–137] these processes have allowed the reduction of surface defects, reduced degradation and prevented oxidation in aqueous solutions and improved dispersability in hybrid organic–inorganic composites. For instance, surface engineering by hybrid plasma-liquid approaches (Figure 2g) has produced important results for Si QDs as the stabilization of the photoluminescence (PL) properties of doped Si QDs could be achieved. More specifically, a high frequency (450 MHz) microplasma jet with argon at 150 sccm was applied to a colloid of Si QDs in ethanol producing an enhancement of the PL quantum yield (QY). Typical absolute PL QY of both p-type and n-type Si QDs, before and after surface engineering, is summarized in Figure 9. The QY of p-type Si QDs is increased from ~10 to 29% and n-type Si QDs QY increased from ~7 to 48%.[138] The significant increment of QY for surface engineered Si QDs is due to the reduction/passivation of surface defects during microplasma processing.

The improvements are attributed to the formation of short organic ligands on the surface of p-type Si QDs and based on Si-O-C_xH_y terminations;[139] n-type Si QDs on the other side, due to electron-rich surfaces, are believed to form a stable oxide shell.[140,141]

While this APP-based surface engineering technique has been widely studied for Si QDs, it is also applicable to a larger range of nanomaterials that include TiO_2 NPs, graphene, and BN nanosheets[142,143] and therefore it is a viable mean to address carriers transport issues. A plasma-liquid approach (Figure 5c), however, is not the only way to tailor interface chemistries and a much wider range of opportunities are possible by combining APP technologies and processes. In particular, the simplicity and atmospheric pressure operation is an advantage that would allow separate processes to co-exist so that materials synthesis and interface engineering can be optimized (e.g., Figure 5d).

5. Introducing Atmospheric Pressure Plasma Processes in Device Fabrication

APPs are not yet used for 3-Gen device fabrication; however, it is clear from this report that materials suitable for PV devices can be reliably produced and that research efforts and technological developments can in principle allow for a

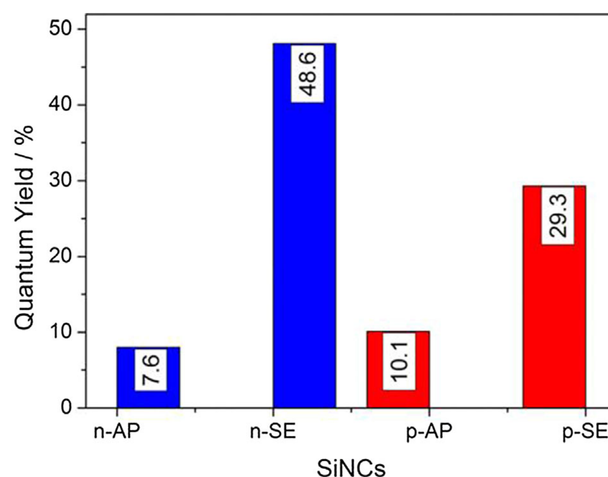

Figure 9. Absolute photoluminescence quantum yield of p- and n-type silicon quantum dots, or silicon nanocrystals (SiNCs) before, i.e., as-prepared (AP) and after surface engineering (SE). Reprinted with permission from ref.[138] Copyright 2016, American Chemical Society.

© 2016 The Authors. *Plasma Processes and Polymers* published by Wiley-VCH Verlag GmbH & Co. KGaA Weinheim

16128869, 2016, 1, Downloaded from https://onlinelibrary.wiley.com/doi/10.1002/ppap.201500187 by Technische Informationsbibliothek, Wiley Online Library on [24/01/2025]. See the Terms and Conditions (https://onlinelibrary.wiley.com/terms-and-conditions) on Wiley Online Library for rules of use; OA articles are governed by the applicable Creative Commons License

wider utilization of APPs first within a research context and then, possibly, for industrial implementation. In this section, we first report on an example of an APP process that has been used to improve 3-Gen device performance. Following, we will describe a first attempt of integrating different APPs in a working 3-Gen device.

An organic device based on a bulk heterojunction is schematically depicted in Figure 10 (left), where the poly(3,4-ethylenedioxythiophene):poly(styrenesulfonate) (PEDOT:PSS) layer represents a water-compatible conductive polymer used to improve the interface between the ITO and the organic active layer formed by polythieno-[3,4-b]thiophenebenzodithiophene (PTB7):[6,6]-phenyl-C71-butyric acid ([70]PCBM). Because of the degradability of organic solar cell under ultra-violet light, a useful recycling scheme for short wavelength radiation is desirable whereby high energy photons can be converted into low energy photons.

A possibility to implement such a scheme is represented by introducing Si NCs somewhere before the active layer so that UV light could be absorbed and re-emitted by the Si NCs PL at longer wavelengths. For instance, a nanocomposite formed with Si NCs and the PEDOT:PSS layer could be inserted as shown in Figure 10 (right), providing an effective down-conversion for blue photons (high energy photons above ~2.7 eV) into red photons (below ~1.8 eV). However, PEDOT:PSS disperses in water while Si NCs do not and degrade in aqueous solution. In order to produce the Si NCs/PEDOT:PSS nanocomposite, an APP-liquid process has been applied to Si NCs/water colloids promoting their long-term stability and improving the QY.[141,144] The APP step has therefore allowed for the fabrication of an organic device with a 3-Gen hybrid converting layer (Figure 10 right) which resulted in an improved performance (Figure 11).

The integration of the nanocomposite in organic devices enhanced the photocurrent generation under concentrated light and prevented UV radiation from reaching the organic active layer, therefore limiting its degradation. Since a higher photon flux of high energy photons increases the Si NCs PL intensity, an enhancement of the optical down-conversion effect should be expected for concentrated light. Figure 11 compares the *J–V* characteristics with 100 mW cm^{-2} (one sun), 200 mW cm^{-2} (two suns), and

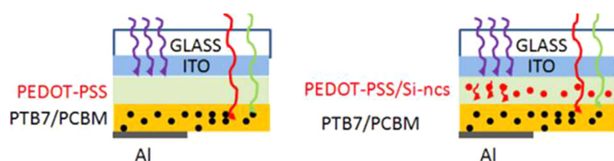

Figure 10. Schematic device structure without (left) and with (right) the silicon nanocrystals (Si-NCs) in the PEDOT:PSS layer.[144] Published by The Royal Society of Chemistry.

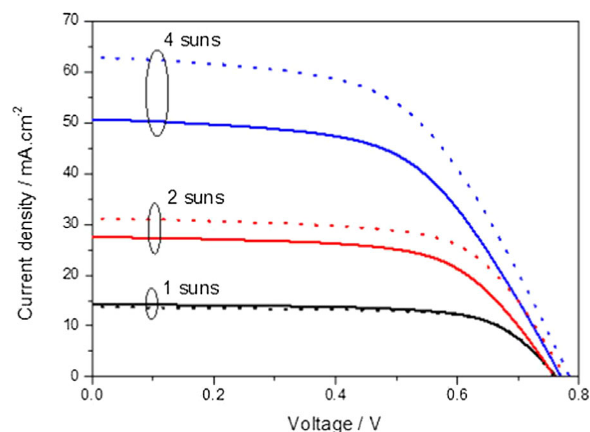

Figure 11. Current density versus voltage (*J–V*) curves of PTB7:PCBM solar cells with (full lines) and without (dotted lines) the Si quantum dots in the PEDOT:PSS layer under irradiation at different levels of concentrated light.[144] Published by The Royal Society of Chemistry.

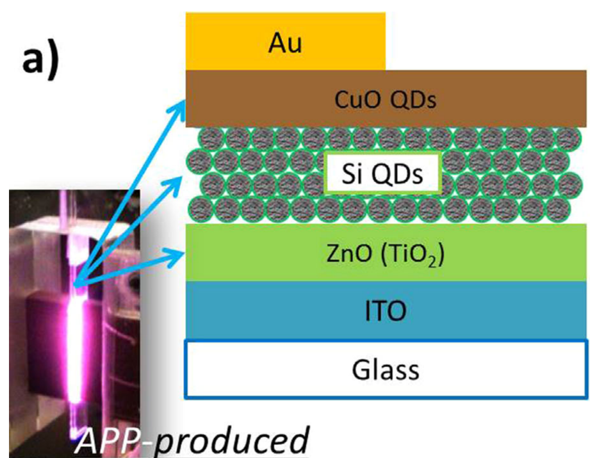

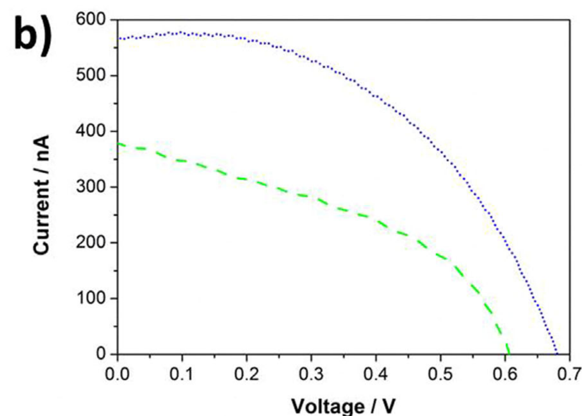

Figure 12. (a) Schematic diagram of device architecture where different materials components could be produced by atmospheric pressure plasmas. (b) Current–voltage characteristic of two devices where two materials component were produced by atmospheric pressure plasmas.

Plasma Process. Polym. **2016,** *13*, 70–90
© 2016 The Authors. *Plasma Processes and Polymers* published by Wiley-VCH Verlag GmbH & Co. KGaA Weinheim
DOI: 10.1002/ppap.201500187

16128869, 2016, 1, Downloaded from https://onlinelibrary.wiley.com/doi/10.1002/ppap.201500187 by Technische Informationsbibliothek, Wiley Online Library on [24/01/2025]. See the Terms and Conditions (https://onlinelibrary.wiley.com/terms-and-conditions) on Wiley Online Library for rules of use; OA articles are governed by the applicable Creative Commons License

16128869, 2016, 1, Downloaded from https://onlinelibrary.wiley.com/doi/10.1002/ppap.201500187 by Technische Informationsbibliothek, Wiley Online Library on [24/01/2025]. See the Terms and Conditions (https://onlinelibrary.wiley.com/terms-and-conditions) on Wiley Online Library for rules of use; OA articles are governed by the applicable Creative Commons License

400 mW cm^{-2} (four suns) irradiance for solar cell without (full lines) and with the Si QDs (dotted lines). Si NCs surface characteristics generally complicate the interactions with polymer matrices. Particularly, interaction with water-soluble polymers such as PEDOT:PSS is challenging since H-terminated Si NCs are hydrophobic. Therefore, the availability of surfactant-free surface-engineered Si NCs produced after the APP treatment, offer excellent opportunities for optimized interactions with polymers leading to solar cell devices with enhanced performance and fabrication processes.

The integration of APPs in the fabrication of 3-Gen devices can be more "invasive." Figure 12a reports the structure of an experimental solar cell device where three (ZnO, Si NCs, and CuO QDs) of the required layers are produced by APPs according to a scheme similar to the one of Figure 5d.

In this device structure, the active layer is represented by the Si QDs while ZnO and CuO QDs represent the transport/blocking layers. Working devices could be produced with a spin-coated TiO_2 thin film where the Si QDs were directly deposited from an APP processes as described above in Section 4.5. The CuO QDs were first synthesized by plasma-liquid synthesis (Figure 2g) and then spray coated (according to scheme of Figure 5c). Figure 12b shows the current–voltage characteristics of two such devices which show good rectification and an open circuit voltage above 0.6 V. While the current is still low and some reproducibility issues have to be resolved, these very first APP-produced devices demonstrate interesting future prospects.

6. Conclusion

APP technologies have achieved great progress in a range of application fields. The use of APPs is, however, still limited in part due to difficulties in competing with well-established low-pressure plasma processes. While APP cannot offer the same features of low-pressure plasma operation, APPs have distinctive characteristics and advantages for a range of new and emerging materials-based technologies. 3-Gen PVs may represent a great opportunity for APPs and vice versa, next generation PVs may gain great benefits from APP materials processing.

While some materials (e.g., oxides) and some configurations/technologies (e.g., DBD) are relatively well advanced and are becoming attractive for a range of industrial applications, other APPs (e.g., hybrid plasma-liquid) and other materials (e.g., QDs) still require much work to become industrially viable. It is therefore difficult to provide a generalized statement on the future of APPs for next generation PVs where such diverse developments exist. Nonetheless, the work carried out so far demonstrates the potential and versatility of APPs and confirm the possibility for APPs to play a key role in a research environment and possibly for future industrial PV manufacturing.

Acknowledgements: All authors acknowledge the support of the Leverhulme Trust (IN-2012-136), EPSRC (EP/K022237/1 and EP/M024938/1), and FP7 (RAPID-ITN-606889). The COST Action TD1208 is also acknowledged for useful interactions and exchanges.

Received: October 13, 2015; Revised: December 9, 2015; Accepted: December 11, 2015; DOI: 10.1002/ppap.201500187

Keywords: atmospheric pressure plasma; nanomaterials; photovoltaics

[1] F. Massines, C. Sarra-Bournet, F. Fanelli, N. Naudé, N. Gherardi, *Plasma Process. Polym.* **2012**, *9*, 1041.
[2] K. H. Becker, B. B. Godfrey, E. E. Kunhardt, M. Laroussi, L. D. Ludeking, A. A. Neuber, E. Schamiloglu, A. J. Woods, *IEEE Trans. Plasma Sci.* **2015**, *43*, 914.
[3] G. Lloyd, G. Friedman, S. Jafri, G. Schultz, A. Fridman, K. Harding, *Plasma Process. Polym.* **2010**, *7*, 194.
[4] G. F. Brown, J. Wu, *Laser Photon. Rev.* **2009**, *3*, 394.
[5] M. Wolf, *Energ. Convers.* **1971**, *11*, 63.
[6] "High-efficiency III-V multijunction solar cells Next Generation PVs," A. Marti, A. Luqueed, Eds., Institute of Physics, London, **2004**.
[7] A. Luque, A. Marti, *Phys. Rev. Lett.* **1997**, *78*, 5014.
[8] V. I. Klimov, S. A. Ivanov, J. Nanda, *Nature* **2007**, *447*, 441.
[9] A. J. Chatten, K. W. J. Barnham, B. F. Buxton, N. J. Ekins-Daukes, M. A. Malik, *Solar Energ. Mater. Solar Cells* **2003**, *75*, 363.
[10] T. Trupke, M. A. Green, P. Würfel, *J. Appl. Phys.* **2002**, *92*, 1668.
[11] B. S. Richards, *Solar Energ. Mater. Solar Cells* **2006**, *90*, 2329.
[12] G. Conibeer, *Mater. Today* **2007**, *10*, 42.
[13] A. J. Nozik, *Chem. Phys. Lett.* **2008**, *457*, 3.
[14] D. Timmerman, I. Izeddin, P. Stallinga, I. N. Yassievich, T. Gregorkiewicz, *Nat. Photon.* **2008**, *2*, 105.
[15] S. Askari, V. Svrcek, P. Maguire, D. Mariotti, *Adv. Mater.* **2015**, *27*, 8011.
[16] D. Mariotti, S. Mitra, V. Švrček, *Nanoscale* **2013**, *5*, 1385.
[17] X. Lan, O. Voznyy, A. Kiani, F. P. G. de Arquer, A. S. Abbas, G.-H. Kim, M. Liu, Z. Yang, G. Walters, J. Xu, M. Yuan, Z. Ning, F. Fan, P. Kanjanaboos, I. Kramer, D. Zhitomirsky, P. Lee, A. Perelgut, S. Hoogland, E. H. Sargent, *Adv. Mater.* in press doi: 10.1002/adma.201503657
[18] D. B. Straus, E. D. Goodwin, E. A. Gaulding, S. Muramoto, C. B. Murray, C. R. Kagan, *J. Phys. Chem. Lett.* **2015**, *6*, 4605.
[19] M. Hossain, D. Hegemann, in *Textile Dyeing*, Chapter 9, P. J. Hauser, Ed., InTech, Rijeka, Croatia **2011**, ISBN: 978-953-307-565-5.
[20] D. Hegemann, in *Comprehensive Materials Processing*, Volume 4. 4.09 – Plasma Polymer Deposition and Coatings on Polymers, S. Hashmi, Ed., Elsevier Ltd., Amsterdam **2014**, ISBN: 978-0-08-096533-8.
[21] J. Park, J. Oh, E. Gil, G. Y. Yeom, *Mater. Res. Bulletin* **2012**, *47*, 3011.

© 2016 The Authors. *Plasma Processes and Polymers* published by Wiley-VCH Verlag GmbH & Co. KGaA Weinheim

[22] G. Y. Kim, J. B. Park, G. Y. Yeom, *J. Korean Phys. Soc.* **2012**, *61*, 397.
[23] J. Vallade, R. Bazinette, L. Gaudy, F. Massines, *J. Phys. D Appl. Phys.* **2014**, *47*, 224006.
[24] T.-H. Wu, I.-C. Cheng, C.-C. Hsu, J.-Z. Chen, *J. Alloys Compd.* **2015**, *628*, 68.
[25] S.-T. Lien, J.-Z. Chen, Y.-J. Yang, C.-C. Hsu, I.-C. Cheng, *Ceram. Int.* **2014**, *40*, 2707.
[26] E. Ritz, Y. L. Wu, J. Hong, D. Andruczyk, T. S. Cho, D. N. Ruzic, *Surf. Coat. Technol.* **2014**, *251*, 64.
[27] W.-Y. Liao, H. Chang, Y.-J. Yang, C.-C. Hsu, I.-C. Cheng, J.-Z. Chen, *Appl. Surf. Sci.* **2014**, *292*, 213.
[28] J. J. Shi, M. G. Kong, *Phys. Rev. Lett.* **2006**, *96*, 105009.
[29] D. Mariotti, R. M. Sankaran, *J. Phys. D Appl. Phys.* **2010**, *43*, 323001.
[30] A. A. Fridman, L. A. Kennedy, in *Plasma Physics and Engineering*, Taylor & Francis, New York **2004**.
[31] K. H. Becker, K. H. Schoenbach, J. G. Eden, *J. Phys. D Appl. Phys.* **2006**, *39*, R55.
[32] F. Iza, G. J. Kim, S. M. Lee, J. K. Lee, J. L. Walsh, Y. T. Zhang, M. G. Kong, *Plasma Process. Polym.* **2008**, *5*, 322.
[33] U. Kogelschatz, *Plasma Chem. Plasma Process.* **2003**, *23*, 1.
[34] L. Bárdos, H. Baránková, *Thin Solid Films* **2010**, *518*, 6705.
[35] C. Tendero, C. Tixier, P. Tristant, J. Desmaison, P. Leprince, *Spectrochim. Acta B* **2006**, *61*, 2.
[36] F. Massines, N. Gherardi, A. Fornelli, S. Martin, *Surf. Coat. Technol.* **2005**, *200*, 1855.
[37] S. A. Starostin, El. Sabbagh-Mansour, E. Aldea, H. de Vries, M. Creatore, M. C. M. van de Sanden, *IEEE Trans. Plasma Sci.* **2008**, *36*, 968.
[38] H. Caquineau, I. Enache, N. Gherardi, N. Naudé, F. Massines, *J. Phys. D Appl. Phys.* **2009**, *42*, 125201.
[39] F. Massines, C. Sarra-Bournet, F. Fanelli, N. Naudé, N. Gherardi, *Plasma Process. Polym.* **2012**, *9*, 1041.
[40] F. Massines, N. Gherardi, in *Recent Progress in Thin Film: Deposition and Characterization*, Research Signpost Ed., Trivandum, India **2010**, Ch. 1.
[41] S. Starostine, E. Aldea, H. de Vries, M. Creatore, M. C. M. van de Sanden, *Plasma Process. Polym.* **2007**, *4*, S440.
[42] S. A. Starostin, M. Creatore, J. B. Bouwstra, M. C. M. van de Sanden, M. de Vries, W. Hindrik, *Plasma Process. Polym.* **2015**, *12*, 545.
[43] M. Cada, O. Churpita, Z. Hubicka, H. Sichova, L. Jastrabík, *Surf. Coat. Technol.* **2004**, *177*, 699.
[44] L. Soukupa, Z. Hubička, A. Churpita, M. Čada, P. Pokorný, J. Zemeka, K. Jureka, L. Jastrabík, *Surf. Coat. Technol.* **2003**, *169*, 571.
[45] S. Stauss, Y. Imanishi, H. Miyazoe, K. Terashima, *Thin Solid Films* **2010**, *518*, 5391.
[46] J. Benedikt, K. Focke, A. Yanguas-Gil, A. von Keudell, *Appl. Phys. Lett.* **2006**, *89*, 251504.
[47] M. D. Barankin, E. Gonzalez II, A. M. Ladwig, R. F. Hicks, *Sol. Energ. Mater. Sol. Cells* **2007**, *91*, 924.
[48] K. W. Johnson, S. Guruvenket, R. A. Sailer, S. P. Ahrenkiel, D. L. Schulz, *Thin Solid Films* **2013**, *548*, 210.
[49] R. A. Sailer, A. Wagner, C. Schmit, N. Klaverkamp, D. L. Schulz, *Surf. Coat. Technol.* **2008**, *203*, 835.
[50] G. R. Nowling, S. E. Babayan, V. Jankovic, R. F. Hicks, *Plasma Sources Sci. Technol.* **2002**, *11*, 97.
[51] M. Thomas, J. Borris, A. Dohse, M. Eichler, A. Hinze, K. Lachmann, K. Nagel, C.-P. Klages, *Plasma Process. Polym.* **2012**, *9*, 1086.
[52] Q. Chen, J. Li, Y. Li, *J. Phys. D Appl. Phys.* **2015**, *48*, 424005.
[53] R. Akolkar, R. M. Sankaran, *J. Vac. Sci. Technol. A* **2013**, *31*, 50811.
[54] A. Lazea-Stoyanova, A. Vlad, A. M. Vlaicu, V. S. Teodorescu, G. Dinescu, *Plasma Process. Polym.* **2015**, *12*, 705.
[55] D. Vollath, *KONA* **2007**, *5*, 39.
[56] P. A. Lin, A. Kumar, R. M. Sankaran, *Plasma Process. Polym.* **2012**, *9*, 1184.
[57] U. Bhandarkar, U. Kortshagen, S. L. Girschick, *J. Phys. D Appl. Phys.* **2003**, *36*, 1399.
[58] J. Patel, L. Nemcova, P. Maguire, W. G. Graham, D. Mariotti, *Nanotechnology* **2013**, *24*, 245604.
[59] W. H. Chiang, C. Richmonds, R. M. Sankaran, *Plasma Source. Sci. Technol.* **2010**, *19*, 034011.
[60] F. C. Chang, C. Richmonds, R. M. Sankaran, *J. Vac. Sci. Technol. A* **2010**, *28*, L5.
[61] C. Richmonds, R. M. Sankaran, *Appl. Phys. Lett.* **2008**, *93*, 131501.
[62] X. Z. Huang, X. X. Zhong, Y. Lu, Y. S. Li, A. E. Rider, S. A. Furman, K. Ostrikov, *Nanotechnology* **2013**, *24*, 095604.
[63] Y. T. Zhang, Y. Guo, T. Ma, *Chin. Phys. Lett.* **2011**, *28*, 105201.
[64] N. Kashihara, H. Setyawan, M. Shimada, *J. Nano. Res.* **2006**, *8*, 395.
[65] X. Liang, Z. J. Wang, C. J. Liu, *Nanoscale Res. Lett.* **2010**, *5*, 124.
[66] I. G. Koo, M. S. Lee, J. H. Shim, *J. Mater. Chem.* **2005**, *15*, 4125.
[67] N. Renaut, M. Jimenez, J. Dutroncy, M. Traisnel, *Thin Solid Films* **2015**, *589*, 161.
[68] Y.-W. Hsu, H.-C. Li, Y.-J. Yang, C.-C. Hsu, *Thin Solid Films* **2011**, *519*, 3095.
[69] C. M. Hsu, S. T. Lien, Y. J. Yang, J. Z. Chen, I. C. Cheng, C. C. Hsu, *Thin Solid Films* **2014**, *570*, 423.
[70] O. V. Penkov, H. J. Lee, V. Y. Plaksin, R. Mansur, J. H. Kim, *Thin Solid Films* **2010**, *518*, 6160.
[71] O. V. Penkov, V. Yu. Plaksin, M. Gook Ko, C. Yim, H.-J. Lee, *J. Korean Phys. Soc.* **2008**, *53*, 2955.
[72] A. Illiberi, F. Grob, C. Frijters, P. Poodt, R. Ramachandra, H. Winands, M. Simor, P. J. Bolt, *Prog. Photovoltaics Res. Appl.* **2013**, *21*, 1559.
[73] M. Watanabe, L. Cui, R. H. Dauskardt, *Org. Electron.* **2014**, *15*, 775.
[74] Y. Ito, O. Sakai, K. Tachibana, *Thin Solid Films* **2010**, *518*, 3513.
[75] Y. Suzaki, S. Ejima, T. Shikama, S. Azuma, O. Tanaka, T. Kajitani, H. Koinuma, *Thin Solid Films* **2006**, *506*, 155.
[76] A.-M. Zhu, L.-H. Nie, Q.-H. Wu, X.-L. Zhang, X.-F. Yang, Y. Xu, C. Shi, *Chem. Vapor Depos.* **2007**, *13*, 141.
[77] L.-B. Di, X.-S. Li, C. Shi, Y. Xu, D.-Z. Zhao, A.-M. Zhu, *J. Phys. D Appl. Phys.* **2009**, *42*, 032001.
[78] S. Kment, P. Kluson, H. Zabova, A. Churpita, M. Chichina, M. Cada, I. Gregora, J. Krysa, Z. Hubicka, *Surf. Coat. Technol.* **2009**, *204*, 667.
[79] H. Chang, Y.-J. Yang, H.-C. Li, C.-C. Hsu, I-C. Cheng, J.-Z. Chen, *J. Power Sources* **2013**, *234*, 16.
[80] T. Yuji, H. Akatsuka, N. Mungkung, B. W. Park, Y. M. Sung, *Vacuum* **2008**, *83*, 124.
[81] R. Maurau, N. D. Boscher, S. Olivier, S. Bulou, T. Belmonte, J. Dutroncy, T. Sindzingre, P. Choquet, *Surf. Coat. Technol.* **2013**, *232*, 159.
[82] N. D. Boscher, S. Olivier, R. Maurau, S. Bulou, T. Sindzingre, T. Belmonte, P. Choquet, *Appl. Surf. Sci.* **2014**, *311*, 721.
[83] V. Shrotriya, G. Li, Y. Yao, C.-W. Chu, Y. Yang, *Appl. Phys. Lett.* **2006**, *88*, 073508.

© 2016 The Authors. *Plasma Processes and Polymers* published by Wiley-VCH Verlag GmbH & Co. KGaA Weinheim
DOI: 10.1002/ppap.201500187

16128869, 2016, 1, Downloaded from https://onlinelibrary.wiley.com/doi/10.1002/ppap.201500187 by Technische Informationsbibliothek, Wiley Online Library on [24/01/2025]. See the Terms and Conditions (https://onlinelibrary.wiley.com/terms-and-conditions) on Wiley Online Library for rules of use; OA articles are governed by the applicable Creative Commons License

[84] G. Li, C.-W. Chu, V. Shrotriya, J. Huang, Y. Yang, *Appl. Phys. Lett.* **2006**, *88*, 253503.
[85] R. P. Cardoso, T. Belmonte, G. Henrion, T. Gries, E. Tixhon, *J. Appl. Phys.* **2010**, *107*, 024909.
[86] A. Lebid, A. Veklich, V. Boretskij, S. Savenok, O. Andreev, *J. Phys.: Conf. Series* **2014**, *550*, 012027.
[87] A. C. Bose, Y. Shimizu, D. Mariotti, T. Sasaki, K. Terashima, N. Koshizaki, *Nanotechnology* **2006**, *17*, 5976.
[88] D. Mariotti, A. C. Bose, K. Ostrikov, *IEEE Trans. Plasma Sci.* **2009**, *37*, 1027.
[89] D. Mariotti, K. Ostrikov, *J. Phys. D Appl. Phys.* **2009**, *42*, 092002.
[90] D. Mariotti, V. Švrček, D. G. Kim, *Appl. Phys. Lett.* **2007**, *91*, 183111.
[91] D. Mariotti, H. Lindström, A. C. Bose, K. K. Ostrikov, *Nanotechnology* **2008**, *19*, 495302.
[92] D. Z. Pai, *J. Phys. D: Appl. Phys.* **2011**, *44*, 174024.
[93] D. Z. Pai, K. K. Ostrikov, S. Kumar, D. A. Lacoste, I. Levchenko, C. O. Laux, *Sci. Rep.* **2013**, *3*, 1221.
[94] T. Belmonte, G. Arnoult, G. Henrion, T. Gries, *J. Phys. D Appl. Phys.* **2011**, *44*, 363001.
[95] T. L. Koh, E. C. O'Hara, M. J. Gordon, *Nanotechnology* **2012**, *23*, 425603.
[96] T. Koh, E. O'Hara, M. J. Gordon, *J. Crystal Growth* **2013**, *363*, 69.
[97] J.-W. Park, B.-K. Kim, H. J. Kim, S. Park, *Thin Solid Films* **2014**, *550*, 114.
[98] R. Y. Korotkov, R. Gupta, P. Ricou, R. Smith, G. Silverman, *Thin Solid Films* **2008**, *516*, 4720.
[99] C. Wang, J.-Z. Chen, *Ceram. Int.* **2015**, *41*, 5478.
[100] K. Johnson, S. Guruvenket, S. Jha, B. Halverson, C. Olson, R. A. Sailer, K. Pokhodnya, D. L. Schulz, **2009**, Atmospheric-pressure plasma deposition of indium tin oxide. In Photovoltaic Specialists Conference (PVSC), 34th IEEE 001806–001810.
[101] Z. Hubička, M. Čada, M. Šícha, A. Churpita, P. Pokorný, L. Soukup, L. Jastrabík, *Plasma Source. Sci. Technol.* **2002**, *11*, 195.
[102] Y.-L. Kuo, Y.-M. Su, J.-Y. Chang, *Thin Solid Films* **2014**, *570*, 215.
[103] U. Ozgur, Y. I. Alivov, C. Liu, A. Teke, M. A. Reshchikov, S. Dogan, V. Avrutin, S. J. Cho, H. Morkoc, *J. Appl. Phys.* **2005**, *98*, 041301.
[104] *Handbook of Photovoltaic Science and Engineering*, S. H. A. Luque, S. Hegedus, Eds., John Wiley & Sons Ltd., Chennai, India **2003**.
[105] *Fundamentals of Solar Cells: Photovoltaic Solar Energy Conversion*, A. L. Fahrenbruch, R. H. Bube, Eds., Academic Press, New York **1983**.
[106] K.-M. Chang, P.-C. Ho, S.-H. Yu, J.-M. Hsu, K.-H. Yang, C.-J. Wu, C.-C. Chang, *Appl. Surf. Sci.* **2013**, *276*, 756.
[107] K.-M. Chang, P.-C. Ho, A. Ariyarit, K.-H. Yang, J.-M. Hsu, C.-J. Wu, C.-C. Chang, *Thin Solid Films* **2013**, *548*, 460.
[108] T.-S. Chou, H.-T. Lin, Y.-Y. Chen, K.-L. Pan, J.-Y. Juang, *Thin Solid Films* **2015**, *594*, 282.
[109] K.-M. Chang, S.-H. Huang, C.-J. Wu, W.-L. Lin, W.-C. Chen, C.-W. Chi, J.-W. Lin, C.-C. Chang, *Thin Solid Films* **2011**, *519*, 5114.
[110] O. E. Semonin, J. M. Luther, S. Choi, H.-Y. Chen, J. Gao, A. J. Nozik, M. C. Beard, *Science* **2011**, *334*, 1530.
[111] J. B. Sambur, T. Novet, B. A. Parkinson, *Science* **2010**, *330*, 63.
[112] A. H. Ip, S. M. Thon, S. Hoogland, O. Voznyy, D. Zhitomirsky, R. Debnath, L. Levina, L. R. Rollny, G. H. Carey, A. Fischer, K. W. Kemp, I. J. Kramer, Z. Ning, A. J. Labelle, K. W. Chou, A. Amassian, E. H. Sargent, *Nat. Nanotechnol.* **2012**, *7*, 577.
[113] E. Thimsen, U. R. Kortshagen, E. S. Aydil, *J. Phys. D Appl. Phys.* **2015**, *48*, 314004.
[114] S. Askari, M. Macias-Montero, T. Velusamy, P. Maguire, V. Svrcek, D. Mariotti, *J. Phys. D Appl. Phys.* **2015**, *48*, 314002.
[115] B. Barwe, A. Stein, O.E. Cibulka, I. Pelant, J. Ghanbaja, T. Belmonte, J. Benedikt, *Plasma Process. Polym.* **2015**, *12*, 132.
[116] B. Barwe, F. Riedel, O. E. Cibulka, I. Pelant, J. Benedikt, *J. Phys. D Appl. Phys.* **2015**, *48*, 314001.
[117] S. Askari, I. Levchenko, K. Ostrikov, P. Maguire, D. Mariotti *Appl. Phys. Lett.* **2014**, *104*, 163103.
[118] A. G. Aberle, R. Hezel, *Prog. Photovolt.* **1997**, *5*, 29.
[119] C. Leguijt, P. Lölgen, J. A. Eikelboom, A. W. Weeber, F. M. Schuurmans, W. C. Sinke, P. F. A. Alkemade, P. M. Sarro, C. H. M. Maree, L. A. Verhoef, *Solar Energ. Mater. Solar Cells* **1996**, *40*, 297.
[120] O. P. Agnihotri, S. C. Jain, J. Poortmans, J. Szlufcik, G. Beaucarne, J. Nijs, R. Mertens, *Semicond. Sci. Technol.* **2000**, *15*, R29.
[121] T. Lauinger, J. Schmidt, A. G. Aberle, R. Hezel, *Appl. Phys. Lett.* **1996**, *68*, 1232.
[122] T. Lauinger, A. G. Aberle, R. Hezel, *Proc. 14th European Photovoltaic Solar Energy Conf.*, Barcelona, Bedford: Stephens, **1997**, 853.
[123] J. Schmidt, M. Kerr, A. Cuevas, *Semicond. Sci. Technol.* **2001**, *16*, 164.
[124] J. D. Moschner, J. Henze, J. Schmidt, R. Hezel, *Prog. Photovoltaics Res. Appl.* **2004**, *12*, 21.
[125] H. Kakiuchi, Y. Nakahama, H. Ohmi, K. Yasutake, K. Yoshii, Y. Mori, *Thin Solid Films* **2005**, *479*, 17.
[126] H. Kakiuchi, H. Ohmi, M. Aketa, K. Yasutake, K. Yoshii, Y. Mori, *Thin Solid Films* **2006**, *496*, 259.
[127] J. Vallade, S. Pouliquen, P. Lecouvreur, R. Bazinette, E. Hernandez, S. Quoizola, F. Massines, *Energ. Procedia* **2012**, *27*, 365.
[128] J. A. Silva, A. Lukianov, R. Bazinette, D. Blanc-Pélissier, J. Vallade, S. Pouliquen, L. Gaudy, M. Lemiti, F. Massines, *Energ. Procedia* **2014**, *55*, 741.
[129] V. Hopfe, D. Rogler, G. Maeder, I. Dani, K. Landes, E. Theophile, M. Dzulko, C. Rohrer, C. Reichhold, *Chem. Vap. Dep.* **2005**, *11*, 510.
[130] V. Hopfe, D. W. Sheel, *Plasma Proc. Polym.* **2007**, *4*, 253.
[131] T. Belmonte, R. P. Cardoso, C. Noël, G. Henrion, F. Kosior, *Eur. Phys. J. Appl. Phys.* **2008**, *42*, 41.
[132] T. Belmonte, T. Gries, R. P. Cardoso, G. Arnoult, F. Kosior, G. Henrion, *Plasma Source. Sci. Technol.* **2011**, *20*, 024004.
[133] P. W. M. Blom, V. D. Mihailetchi, L. J. A. Koster, D. E. Markov, *Adv. Mater.* **2007**, *19*, 1551.
[134] N. Mukherjee, D. Wavhal, R. B. Timmons, *ACS Appl. Mater. Interf.* **2010**, *2*, 397.
[135] V. Švrcek, M. Kondo, K. Kalia, D. Mariotti, *Chem. Phys. Lett.* **2009**, *478*, 224.
[136] V. Švrček, D. Mariotti, M. Kondo, *Appl. Phys. Lett.* **2010**, *97*, 161502.
[137] V. Svrcek, D. Mariotti, Y. Shibata, M. Kondo, *J. Phys. D Appl. Phys.* **2010**, *43*, 415402.
[138] T. Velusamy, S. Mitra, M. Macias-Montero, V. Svrcek, D. Mariotti, *ACS Appl. Mater. Interf.* **2015**, DOI: 10.1021/acsami.5b06577.
[139] D. Mariotti, V. Švrcek, J. W. J. Hamilton, M. Schmidt, M. Kondo, *Adv. Funct. Mater.* **2012**, *22*, 954.

© 2016 The Authors. *Plasma Processes and Polymers* published by Wiley-VCH Verlag GmbH & Co. KGaA Weinheim

16128869, 2016, 1, Downloaded from https://onlinelibrary.wiley.com/doi/10.1002/ppap.201500187 by Technische Informationsbibliothek, Wiley Online Library on [24/01/2025]. See the Terms and Conditions (https://onlinelibrary.wiley.com/terms-and-conditions) on Wiley Online Library for rules of use; OA articles are governed by the applicable Creative Commons License

[140] S. Mitra, V. Svrcek, D. Mariotti, T. Velusamy, K. Matsubara, M. Kondo, *Plasma Process. Polym.* **2014**, *11*, 158.
[141] S. Mitra, S. Cook, V. Svrcek, R. A. Blackley, W. Zhou, J. Kovac, U. Cvelbar, D. Mariotti, *J. Phys. Chem. C.* **2013**, *117*, 23198.
[142] J. McKenna, J. Patel, S. Mitra, N. Soin, V. Svrcek, P. Maguire, D. Mariotti, *Eur. Phys. J. Appl. Phys.* **2011**, *56*, 24020.
[143] Y. Liu, D. Sun, S. Askari, J. Patel, M. Macias-Montero, S. Mitra, R. Zhang, W.-F. Lin, D. Mariotti, P. Maguire, *Sci. Rep.* **2015**, *5*, 15765.
[144] V. Svrcek, T. Yamanari, D. Mariotti, S. Mitra, T. Velusamy, K. Matsubara, *Nanoscale* **2015**, *7*, 11566.
[145] J. Vallade, S. Pouliquen, P. Lecouvreur, R. Bazinette, E. Hernandez, S. Quoizola, F. Massines, *Energ. Procedia* **2012**, *27*, 365.
[146] J. A. Silva, A. Lukianov, R. Bazinette, D. Blanc-Pélissier, J. Vallade, S. Pouliquen, L. Gaudy, M. Lemiti, F. Massines, *Energ. Procedia* **2014**, *55*, 741.
[147] T. L. Koh, M. J. Gordon, *J. Vacuum Sci. Technol. A* **2013**, *31*, 061312.

© 2016 The Authors. *Plasma Processes and Polymers* published by Wiley-VCH Verlag GmbH & Co. KGaA Weinheim
DOI: 10.1002/ppap.201500187

16128869, 2016, 1, Downloaded from https://onlinelibrary.wiley.com/doi/10.1002/ppap.201500187 by Technische Informationsbibliothek, Wiley Online Library on [24/01/2025]. See the Terms and Conditions (https://onlinelibrary.wiley.com/terms-and-conditions) on Wiley Online Library for rules of use; OA articles are governed by the applicable Creative Commons License